Inorganic Chemistry
Article
Cite This: Inorg. Chem. XXXX, XXX, XXX−XXX
pubs.acs.org/IC

Synthetic Model Complex of the Key Intermediate in Cytochrome P450 Nitric Oxide Reductase

Ashley B. McQuarters,[†] Elizabeth J. Blaesi,[‡] Jeff W. Kampf,[†] E. Ercan Alp,[§] Jiyong Zhao,[§] Michael Hu,[§] Carsten Krebs,[‡] and Nicolai Lehnert*[,†]

[†]Department of Chemistry and Department of Biophysics, University of Michigan, Ann Arbor, Michigan 48109, United States
[‡]Department of Chemistry and Department of Biochemistry and Molecular Biology, The Pennsylvania State University, University Park, Pennsylvania 16802, United States
[§]Advanced Photon Source (APS), Argonne National Laboratory (ANL), Argonne, Illinois 60439, United States

Supporting Information

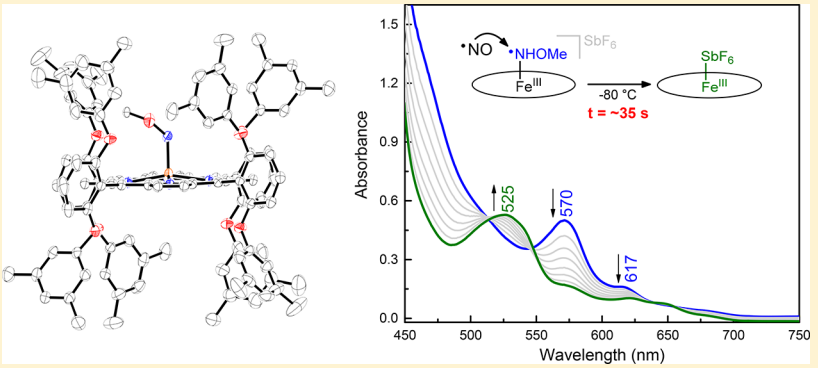

ABSTRACT: Fungal denitrification plays a crucial role in the nitrogen cycle and contributes to the total N_2O emission from agricultural soils. Here, cytochrome P450 NO reductase (P450nor) reduces two NO to N_2O using a single heme site. Despite much research, the exact nature of the critical "Intermediate I" responsible for the key N−N coupling step in P450nor is unknown. This species likely corresponds to a Fe-NHOH-type intermediate with an unknown electronic structure. Here we report a new strategy to generate a model system for this intermediate, starting from the iron(III) methylhydroxylamide complex [Fe(3,5-Me-BAFP)(NHOMe)] (**1**), which was fully characterized by ^{1}H NMR, UV−vis, electron paramagnetic resonance, and vibrational spectroscopy (rRaman and NRVS). Our data show that **1** is a high-spin ferric complex with an N-bound hydroxylamide ligand that is strongly coordinated (Fe−N distance, 1.918 Å; Fe-NHOMe stretch, 558 cm^{-1}). Simple one-electron oxidation of **1** at −80 °C then cleanly generates the first model system for Intermediate I, $[Fe(3,5\text{-}Me\text{-}BAFP)(NHOMe)]^+$ ($\mathbf{1}^+$). UV−vis, resonance Raman, and Mössbauer spectroscopies, in comparison to the chloro analogue $[Fe(3,5\text{-}Me\text{-}BAFP)(Cl)]^+$, demonstrate that $\mathbf{1}^+$ is best described as an Fe^{III}-$(NHOMe)^{\bullet}$ complex with a bound NHOMe radical. Further reactivity studies show that $\mathbf{1}^+$ is highly reactive toward NO, a reaction that likely proceeds via N−N bond formation, following a radical−radical-type coupling mechanism. Our results therefore provide experimental evidence, for the first time, that an Fe^{III}-$(NHOMe)^{\bullet}$ electronic structure is indeed a reasonable electronic description for Intermediate I and that this electronic structure is advantageous for P450nor catalysis because it can greatly facilitate N−N bond formation and, ultimately, N_2O generation.

INTRODUCTION

Nitrogen is an essential building block for all forms of life on Earth.[1−3] The primary sources of nitrogen for plants are ammonia (NH_3/NH_4^+) and nitrate (NO_3^-; from minerals). Ammonia is generated from dinitrogen (N_2) through biological (nitrogenases) and synthetic (the Haber−Bosch process) nitrogen fixation and then utilized by plants. However, plants only use a fraction of the ammonia that is provided by fertilization of agricultural soils, and the remainder is metabolized by large microbial communities that live in the soil and seawater. Ammonia is oxidized by nitrifying microbes to nitrite (NO_2^-) and nitrate (NO_3^-), which are then picked up by denitrifying bacteria and fungi, which reduce NO_3^- stepwise to nitrous oxide (N_2O; nar = nitrate reductase; nir = nitrite reductase; nor = nitric oxide reductase):[4,5]

$$NO_3^- \xrightarrow{nar} NO_2^- \xrightarrow{nir} {}^{\bullet}NO \xrightarrow{nor} N_2O \qquad (1)$$

In the final step of denitrification (not shown above), N_2O is further reduced to N_2 (by denitrifying bacteria only) to close the nitrogen cycle. Overfertilization of agricultural soil has

Received: October 17, 2018

DOI: 10.1021/acs.inorgchem.8b02947
Inorg. Chem. XXXX, XXX, XXX−XXX

become a common practice in the developed world (to ensure that nitrogen is never a limiting nutrient for crop growth), which leads to an overabundance of bioavailable nitrogen.[6,7] As a result, denitrifying bacteria and fungi metabolize increasing amounts of NO_3^-/NO_2^- and release steadily increasing quantities of the gaseous intermediates NO and N_2O into the atmosphere. This is a major environmental concern because both NO and N_2O deplete the ozone layer and N_2O is also a potent greenhouse gas.[7] These environmental impacts have led to great interest in the enzymes involved in nitrification and denitrification and their catalytic mechanisms.[8]

One enzyme involved in the two-electron reduction of NO to N_2O that prevents accumulation of this toxic metabolite is cytochrome P450 nitric oxide reductase (P450nor).[9,10] This enzyme is found in soil-dwelling, denitrifying fungi like the ubiquitous *Fusarium oxysporum* but also yeasts (for example, *Trichosporon cutaneum*). P450nor belongs to the cytochrome P450 superfamily (Cyt. P450s), which are enzymes that mostly perform oxidative (especially monooxygenase) chemistry. Unlike the typical Cyt. P450s, P450nor is unique for its function as a reductase, even though the active site of P450nor shares strong structural similarities with its monooxygenase counterparts, in particular the single heme *b* with a proximal (axial) cysteinate ligand.[11,12] Figure 1 shows the crystal

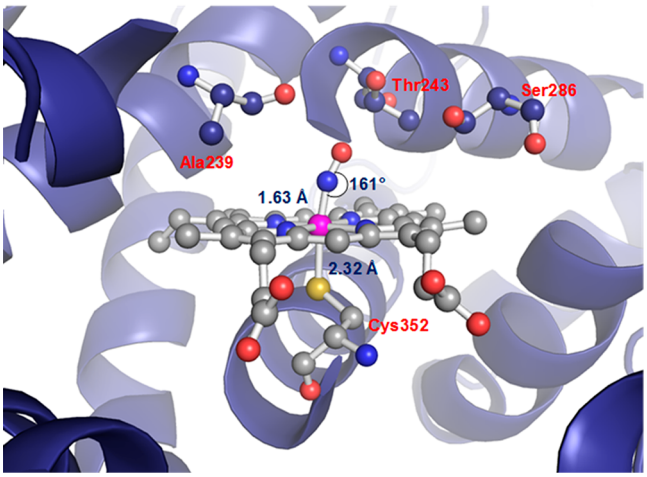

Figure 1. NO-bound ferric heme in the active site of P450nor from *F. oxysporum*. This image was generated using *PyMol* from PDB code 1CL6 (adapted from ref 13).

structure of the NO-bound ferric heme complex of *F. oxysporum* P450nor.[13] This enzyme performs NO reduction following eq 2 with a turnover frequency of ~1200 s^{-1}. The necessary electrons are derived from NAD(P)H without the aid of an electron-transfer protein.[14]

$$2NO + NAD(P)H + H^+ \rightarrow N_2O + H_2O + NAD(P)^+ \quad (2)$$

In the first step of catalysis, the ferric heme complex of P450nor binds NO to form a ferric heme nitrosyl, or $\{FeNO\}^6$ complex in the Enemark–Feltham notation (where the superscript "6" represents the number of Fe(d) electrons plus the NO(π^*) electrons),[15] as the first intermediate of the reaction.[16,17] NO binding goes along with a shift of the Soret band from 413 to 431 nm.[17] The NO complex is further characterized by N–O and Fe–NO stretching frequencies of 1851 and 530 cm^{-1}, respectively.[18] This is followed by a direct hydride transfer from NAD(P)H to the heme-$\{FeNO\}^6$ complex.[11] This reaction causes a characteristic change in the Soret band, which shifts from 431 to 444 nm.[17] The lifetime of the resulting "Intermediate I" is only 100 ms, making it difficult to further study this species. From resonance Raman (rRaman) spectroscopy, the Fe–NO stretching frequency of this intermediate is 596 cm^{-1}.[19] On the basis of the above reaction sequence, Intermediate I corresponds to a nitroxyl level complex of the type $\{FeN(H)_nO\}^8$ (n = 0–2) of an unknown protonation state. Density functional theory (DFT) and quantum mechanics/molecular mechanics (QM/MM) calculations have helped to shed further light on the details of the reaction.[20,21] From DFT, the $\{FeNO\}^6$ complex is best described as an Fe^{II}-NO^+ species, which is consistent with its spectroscopic properties (see above). Direct hydride transfer from NAD(P)H initially generates a ferrous heme-HNO species, as shown in Scheme 1, which is very likely N-protonated [based on (a) total energy considerations from DFT[20] and (b) the experimental findings for the myoglobin(II)-NHO adduct[22]]. At this point, the ferrous heme-NHO species could react directly with a second equiv of NO to form the N–N bond and generate a ferric hyponitrite intermediate. Alternatively, because of the strong donicity of the cysteinate ligand, the ferrous HNO complex could be further protonated, resulting in a formally Fe^{IV}-$NHOH^-$ species.[20] On the basis of recent QM/MM calculations, the electronic structure of this intermediate could also be described as an Fe^{III}-$(NHOH)^\bullet$ complex, where a NHOH radical is bound to a low-spin (ls) iron(III) and the spins are antiferromagnetically coupled (total spin S = 0).[21] Then, the subsequent addition of NO generates again a ferric hyponitrite complex, which readily decomposes into N_2O and H_2O, closing the catalytic cycle (see Scheme 1). On the basis of these results, the critical Intermediate I is identified with either the ferrous heme-NHO complex or the corresponding doubly protonated species.

There is some further experimental evidence that suggests that Intermediate I might be the doubly protonated species. Pulsed radiolysis of hydroxylamine (NH_2OH) was shown to generate the $(NHOH)^\bullet$ radical in water.[23] The irradiation of NH_2OH in the presence of ferric P450nor forms a species with a UV–vis spectrum identical with that of Intermediate I (Soret band at 444 nm).[11] This result implies that Intermediate I is an NHOH-type complex. Further experimental information about this species comes from recent magnetic circular dichroism (MCD) and Mössbauer studies.[24] First, the MCD data of Intermediate I show no paramagnetic MCD *C*-term signal at the Soret band position of this species (445 nm, ~22500 cm^{-1}), which provides direct evidence that Intermediate I is diamagnetic.[25] These results were confirmed by ^{57}Fe Mössbauer spectroscopy. Interestingly, the isomer shift (δ) determined for Intermediate I is within the range for ls ferric hemes ($\delta \approx 0.15$–0.25 mm/s). Unfortunately, no Mössbauer data are available for ferrous heme-NHO complexes for comparison. DFT-calculated isomer shifts are similar for the ferrous heme-NHO (δ = 0.26 mm/s) and Fe^{III}-$(NHOH)^\bullet$ (δ = 0.23 mm/s) complexes, so the protonation state of Intermediate I cannot be assigned based on these results. However, the DFT calculations do not favor the Fe^{IV}-$NHOH^-$ valence tautomer (predicted δ = 0.09 mm/s). In summary, the protonation state and electronic structure of the key intermediate in P450nor catalysis, Intermediate I, are still not

DOI: 10.1021/acs.inorgchem.8b02947
Inorg. Chem. XXXX, XXX, XXX–XXX

Scheme 1. Proposed Mechanism for N_2O Production by P450nor[a]

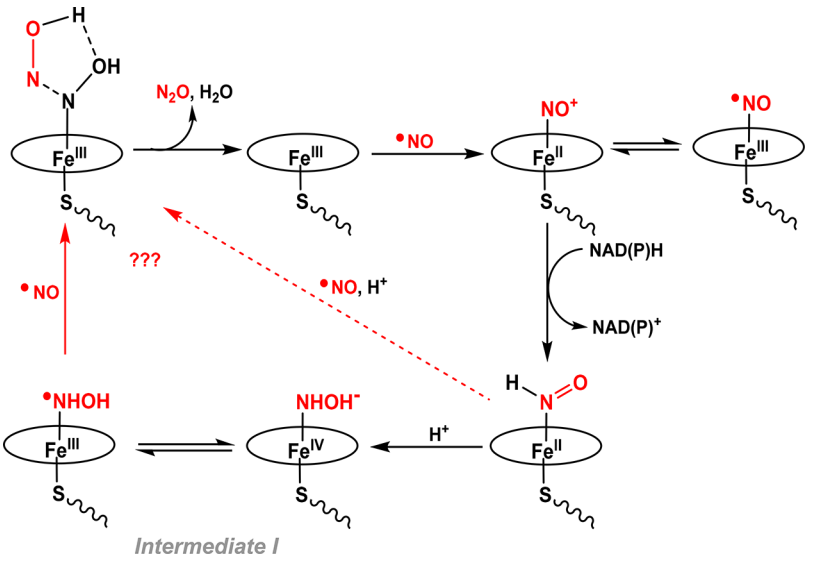

[a]The oval represents a generic porphyrin ligand.

resolved. Therefore, it is the goal of this work to use simple synthetic models to further elucidate the nature, electronic structure, and reactivity of this species.

In this work, we devised a convenient route to synthesize an Fe^{III}-$(NHOR)^{\bullet}$/Fe^{IV}-$NHOR^{-}$-type model complex for Intermediate I through one-electron oxidation of a corresponding Fe^{III}-$NHOR^{-}$ precursor, as shown in Scheme 2. We first

Scheme 2. Synthetic Route Used To Generate a Model for Intermediate I of P450nor

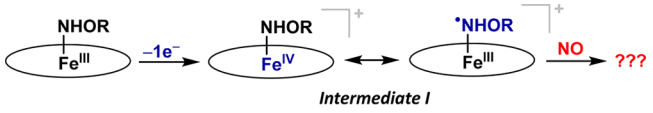

prepared the precursor [Fe(3,5-Me-BAFP)(NHOMe)] (**1**) and fully characterized this complex by UV–vis, ^{1}H NMR, and electron paramagnetic resonance (EPR) spectroscopy, and X-ray crystallography (which represents the first crystal structure of a ferric heme hydroxylamide complex reported to date). Because of the fact that iron(IV) porphyrins are known to be highly reactive, a bis(picket fence) porphyrin, 3,5-Me-$BAFP^{2-}$ ($3,5$-Me-$BAFP^{2-}$ = tetra[2,6-bis(3,5-dimethylphenoxy)-phenyl]porphyrin dianion), was used here to protect the bound hydroxylamide ligand (see Scheme 3). The one-electron oxidation of the Fe^{III}-$NHOMe^{-}$ precursor via chemical oxidation results in the target complex [Fe(3,5-Me-BAFP)(NHOMe)]$^+$ (**1**$^+$), which is a metastable species at −80 °C. We then investigated the spectroscopic properties of this species, using EPR, rRaman, and Mössbauer spectroscopies, which ultimately shows that this intermediate is best described as an Fe^{III}-$(NHOMe)^{\bullet}$ complex and not the Fe^{IV} valence tautomer. This species can be generated in ∼85% yield in solution. Finally, the reactivity of this intermediate with NO was investigated, which leads to the fast generation of a ferric product complex. The implications of these results for the mechanism of P450nor are finally discussed. Note that, compared to the P450nor active site, our model system lacks the axial thiolate ligand, which might further influence the reactivity of Intermediate I in the enzyme. Similar to the

Scheme 3. Target Complex 1, Which Serves as a Precursor for the Proposed Fe^{III}-$(NHOH)^{\bullet}$/Fe^{IV}-$NHOH^{-}$ Intermediate in the Catalytic Cycle of P450nor[a]

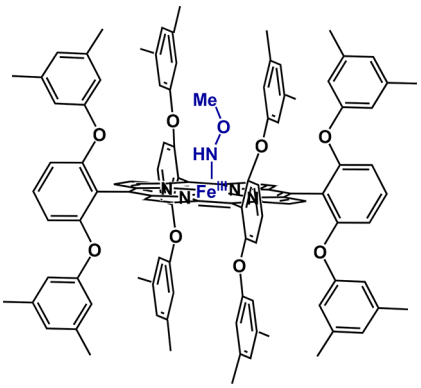

[a]See also Figure 3.

protein matrix, the sterically demanding pickets used in our model provide shielding for reactive intermediates that are coordinated to the heme.

EXPERIMENTAL PROCEDURES

All reactions were performed under inert conditions using Schlenk techniques. The preparation and handling of air-sensitive materials was carried out under a dinitrogen atmosphere in an MBraun glovebox equipped with a circulating purifier (O_2, H_2O < 0.1 ppm). Nitric oxide (Cryogenic Gases Inc., 99.5%) was purified by passage through an ascarite II column (NaOH on silica), followed by a cold trap at −80 °C to remove higher-order nitrogen oxide impurities. All solvents (including deuterated solvents) and 1-methylimidazole were distilled from CaH_2 under dinitrogen and then degassed via five freeze–pump–thaw cycles. Tetrabutylammonium hexafluorophosphate was recrystallized from ethanol. The purified solvents were stored over appropriately sized activated molecular sieves in the glovebox until used. 1,1′-Diacetylferrocene was purchased from Fisher Scientific, tris(4-bromophenyl)ammoniumyl hexachloroantimonate was purchased from Sigma-Aldrich, and *O*-methylhydroxylamine hydrochloride was purchased from TCI America. All of these materials were used without further purification. Deprotonation of

DOI: 10.1021/acs.inorgchem.8b02947
Inorg. Chem. XXXX, XXX, XXX–XXX

O-methylhydroxylamine to the corresponding lithium salt, Li[NHOMe], was carried out as previously reported.[26] [Fe(3,5-Me-BAFP)(Cl)],[27] [Fe(3,5-Me-BAFP)(X)][28] where X = PF_6^- or SbF_6^-, [Co(TPP)],[29] and [DAcFc][SbF_6][30] were synthesized as previously reported. ^{57}Fe complexes were synthesized in the same way as the natural abundance complexes, using $^{57}FeCl_2$ dimethanol salt as the iron source. In this work, NO gas was added to reactions via a syringe from a bomb flask or in a stoichiometric manner using a NO-saturated solution. NO-saturated solutions were prepared under a dinitrogen atmosphere by equilibration of dichloromethane with NO gas in a Schlenk flask. The concentration of the NO gas in the solution was subsequently determined with [Co(TPP)]. The titration of [Co(TPP)] with NO(g)/CH_2Cl_2 was carried out in tetrahydrofuran (THF) and monitored by UV−vis spectroscopy (λ_{max} of the Q band changes from 527 to 537 nm). Typical NO gas concentrations in dichloromethane prepared in this way were ∼1 mM.

Physical Measurements. IR spectra were obtained from KBr disks with PerkinElmer BX and GX spectrometers at room temperature. Electronic absorption spectra were measured using an Analytic Jena Specord S600 instrument at room temperature. EPR spectra were recorded with a Bruker X-band EMX spectrometer equipped with Oxford Instruments liquid-nitrogen and -helium cryostats. EPR spectra were typically obtained on frozen solutions using 20 mW microwave power and 100 kHz field modulation with the amplitude set to 1 G. Sample concentrations were ∼0.1−2 mM. ^{1}H and ^{19}F NMR spectra were recorded on Varian MR 400 MHz and NMRS 500 MHz instruments at room temperature. In situ UV−vis measurements were conducted using a Hellma quartz immersion probe with a 10 mm path length. Mass spectrometry (MS) data were collected on an Agilent 6230 time-of-flight high-performance liquid chromatography/mass spectrometer. Cyclic voltammograms were obtained with a CH instruments CHI600E electrochemical workstation using a three-component system consisting of a glassy carbon working electrode, a platinum counter electrode, and a silver wire pseudoreference electrode. All potentials were corrected to Fc^+/Fc. UV−vis spectroelectrochemical (SEC) measurements were performed using a custom-built thin-layer electrochemical cell as previously described.[27] All electrochemical and SEC measurements were carried out in the presence of ∼0.1 M tetrabutylammonium hexafluorophosphate. Nuclear resonance vibrational spectroscopy (NRVS) measurements were carried out as previously described[31] at beamline 3-ID-XOR at the APS at ANL. This beamline provides about 2.5 × 10^9 photons/s in ∼1 meV bandwidth (8 cm^{-1}) at 14.4125 keV in a 0.5 mm (vertical) × 0.5 mm (horizontal) spot. Samples were loaded into 4 × 7 × 1 mm copper cells. The final spectra represent the averages of four scans. The program *Phoenix* was used to convert the NRVS raw data to the vibrational density of states (VDOS).[32,33] The rRaman measurements were performed using the 413.13 nm excitation line from a Kr^+-ion laser (Spectra Physics Beam Lok 2060-RS). Raman spectra were recorded at 77 K using an Acton two-stage TriVista 555 monochromator connected to a liquid-nitrogen-cooled CCD camera (Princeton Instruments Spec-10:400B/LN). The total exposure time of the samples to the laser radiation was 3 min, using 1−2 accumulations, and typical laser powers were in the 17−30 mW range.

Mössbauer Spectroscopy. Mössbauer data were recorded on a spectrometer from WEB Research, equipped with a Janis SVT-400 variable-temperature cryostat. All isomer shifts are quoted relative to the centroid of the spectrum of α-Fe at room temperature. Simulation of the Mössbauer spectra was conducted with the *WMOSS* spectral analysis package, using the spin Hamiltonian shown in the following equation:

$$H = \beta S\cdot g\cdot B + D\left(S_z^2 - \frac{S(S+1)}{3}\right) + E(S_x^2 - S_y^2) + \frac{eQV_{zz}}{4}\left[I_z^2 - \frac{I(I+1)}{3} + \frac{\eta}{3}(I_x^2 - I_y^2)\right] + S\cdot A\cdot I - g_n\beta_n B\cdot I$$

The first three terms represent the electronic Zeeman effect and zero-field splitting, the fourth term describes the interaction between the nuclear quadrupole moment and electric field gradient, the fifth term represents the magnetic hyperfine interaction of the electronic spin with the ^{57}Fe nucleus, and the last term describes the ^{57}Fe nuclear Zeeman effect.

Crystal Structure Determination of 1. A brown plate of **1** of dimensions 0.22 × 0.15 × 0.02 mm was mounted on a Rigaku AFC10K Saturn 944+ CCD-based X-ray diffractometer equipped with a low-temperature device and a Micromax-007HF copper-target microfocus rotating anode (λ = 1.54187 Å), operated at 1.2 kW power (40 kV, 30 mA). The X-ray intensities were measured at 85 K, with the detector placed at a distance of 42.00 mm from the crystal. A total of 3461 images were collected with an oscillation width of 1.0° in *w*. The exposure time was 5 s for the low-angle images and 20 s for the high-angle images. Rigaku d*trek images were exported to *CryAlisPro*[34] and corrected for absorption. The integration of the data yielded a total of 61858 reflections to a maximum 2θ value of 147.92°, of which 9532 were independent and 8139 were greater than 2$\sigma(I)$. The final cell constants in Table S2 are based on the *xyz* centroids of 17282 reflections above 10$\sigma(I)$. Analysis of the data showed negligible decay during data collection; the data were processed with *CrystalClear 2.0*[35] and corrected for absorption. The structure was solved and refined with the Bruker *SHELXTL* (version 2016/6) software package,[36] using the space group $P\bar{1}$ with Z = 1 for the formula $C_{110}H_{100}N_6O_{10}Fe$. All non-hydrogen atoms were refined anisotropically, with the hydrogen atoms placed in idealized positions. Full matrix least-squares refinement based on F^2 converged at R1 = 0.0957 and wR2 = 0.2816 [based on $I > 2\sigma(I)$] and R1 = 0.1028 and wR2 = 0.2938 for all data.

DFT Calculations. The structure of [Fe(P)(NHOMe)] (P^{2-} = porphine dianion) was fully optimized for the sextet ($S = {}^5/_2$) ground state of complex **1**, using the BP86 functional[37,38] and the TZVP basis set.[39,40] Vibrational frequencies calculated for the optimized structure show no imaginary frequencies. In all calculations, convergence was reached when the relative change in the density matrix between subsequent iterations was less than 1 × 10^{-8}. All of these calculations were performed using the program package *Gaussian 09*.[41]

Preparation of Salt-Free *O*-Methylhydroxylamine. A total of 11.2 g of *O*-methylhydroxylamine hydrochloride (0.134 mmol) was dissolved in 95 mL of a sodium hydroxide solution (5 M). Then, the product *O*-methylhydroxylamine was distilled off under dinitrogen as a clear oil. Yield: 4.53 g (0.096 mol, 72%). ^{1}H NMR ($CDCl_3$, 400 MHz): δ: 3.554 (s, 3H), 5.437 (b, 2H).

Synthesis of [Fe(3,5-Me-BAFP)(NHOMe)] (1). Under an inert atmosphere, 244 mg of [Fe(3,5-Me-BAFP)(PF_6)] (0.137 mmol) was dissolved in 5 mL of dry 2-methyltetrahydrofuran (2-Me-THF; the reaction also works in toluene). Then, 22 mg of Li[NHOMe] (0.75 mmol) was added to the solution, and the reaction was allowed to stir until it looked complete by UV−vis spectroscopy. On the basis of UV−vis conversion, more ligand can be added (typically up to an additional ∼5 equiv) because of the poor solubility of the lithium salt. Typical reaction times are about 24 h. The resulting solution was filtered through a 0.2 μM PTFE filter, layered with hexanes, and allowed to precipitate in the −33 °C freezer. After 2 days, the reaction was filtered through a frit to give a dark-purple powder. Yield: 185 mg (0.110 mmol, 81%). UV−vis (2-Me-THF): 421, 582, 631 nm. UV−vis (toluene): 424, 582, 632 nm. ^{1}H NMR (CD_2Cl_2, 400 MHz): δ −0.887 (b), −3.77 (b), 1.843 (b), 6.172 (b), 6.539 (b), 7.558 (b), 10.285 (b), 11.074 (b), 79.41 (b). Satisfactory elemental analysis required the inclusion of a solvent-derived 2-Me-THF molecule. The reported analysis is for **1**·2-Me-THF. Anal. Calcd for $C_{114}H_{106}FeN_5O$: C, 77.71; H, 6.06; N, 3.97. Found: C, 77.05; H, 5.87; N, 3.21.

The same procedure was followed when using the precursor [Fe(3,5-Me-BAFP)(X)] with X = ClO_4^- or SbF_6^-.

Brown plates suitable for X-ray diffraction were grown by layering a concentrated 2-Me-THF solution of **1** in a 5-mm-diameter glass tube with pentane at room temperature for 3 days.

Chemical Oxidation of [Fe(3,5-Me-BAFP)(Cl)]. Under an inert atmosphere, 7.2 mg of [Fe(3,5-Me-BAFP)(Cl)] (0.0043 mmol) was

DOI: 10.1021/acs.inorgchem.8b02947
Inorg. Chem. XXXX, XXX, XXX−XXX

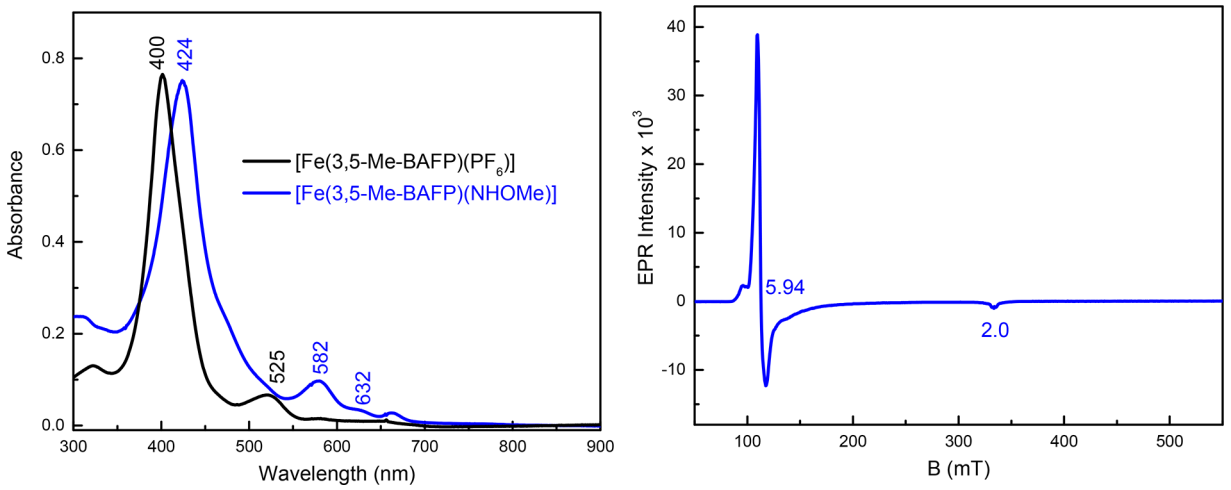

Figure 2. Left: UV−vis spectra of [Fe(3,5-Me-BAFP)(PF_6)] (black) and of the isolated product **1** (blue) in 2-Me-THF at room temperature. Right: EPR spectrum of **1** in toluene at 6 K.

dissolved in 2 mL of dry dichloromethane. The solution was added to 5.6 mg of solid [$N(C_6H_4Br\text{-}4)_3$][$SbCl_6$] (0.0068 mmol) and agitated until all of the solid had dissolved, forming [Fe(3,5-Me-BAFP)(Cl)]-$SbCl_6$. Typical concentrations were in the 1−2 mM range. UV−vis (CH_2Cl_2): 373, 411, 568, 634 nm. ^{1}H NMR (CD_2Cl_2, 500 MHz): δ −10.22 (s), −11.00 (s), 2.34 (b), 7.97 (b), 8.49 (b), 9.11 (b), 15.64 (s), 83.08 (b).

Chemical Oxidation of 1. Typical concentrations of **1** used for these experiments were from ∼5 μM to 0.3 mM, and ∼1−1.5 equiv of the oxidant [DAcFc][SbF_6] was employed. Under an inert atmosphere, a stirring, dry toluene solution of **1** in a custom-designed flask fitted with a UV−vis immersion probe (without its metal casing) was cooled to −80 °C in a dry ice/hexanes bath. The syringes, needles, and oxidant solution were prechilled in dry ice. The oxidant [DAcFc][SbF_6] was dissolved in cold dimethoxyethane (DME; typical concentrations were ∼1 mM) and slowly added to the toluene solution of **1**. Correspondingly, DME reached up to 20% of the total volume of the solution at the highest concentrations of **1** employed. Completion of the reaction to yield the oxidized species $\mathbf{1}^+$ was monitored by in situ UV−vis spectroscopy. Then, this solution was transferred to precooled quartz tubes (in a Dewar with a dry ice/hexanes bath) for EPR and rRaman measurements. For preparation of the samples for Mössbauer spectroscopy, the plastic cup sample holders were cooled inside a custom-designed aluminum block that contained dry ice.

N_2O Detection. Under an inert atmosphere, a stirring, dry toluene solution of **1** in a custom-designed airtight flask fitted with an in situ UV−vis immersion probe (without its metal cover) was cooled to −80 °C in a dry ice/hexanes bath. After oxidation of the complex, NO gas (from a bomb flask; 2−5 mL) was added to a solution of $\mathbf{1}^+$ at −80 °C via a syringe. The reaction progress was monitored using in situ UV−vis spectroscopy, applying the kinetics program of the *Analytic Jena* software package. Once the spectral features of the oxidized species [Fe(3.5-Me-BAFP)(NHOMe)]$^+$ had disappeared (typical reaction times are less than 1 min), the solution was warmed up to room temperature, which took about 30 min. At this point, the UV−vis spectrum looked like that of the six-coordinate (6C) ferric heme nitrosyl complex. The headspace of the flask was then transferred via cannula into a gas IR cell and tested for N_2O.

RESULTS AND ANALYSIS

Synthesis and Characterization of 1. Surprisingly, there are no reports of stable Fe^{III}-NHOH-type complexes, which is likely due to the thermal instability of NH_2OH itself[42,43] and its propensity to disproportionate when reacted with metal centers.[44−46] To increase the stability of NH_2OH, we decided to use a derivative where the oxygen atom of the NH_2OH ligand is bound to a methyl group (NH_2OMe), leading to a room-temperature-stable hydroxylamine derivative. This approach has the additional advantage that the methyl substituent will help direct the nitrogen atom to bind to the iron center, generating the target complex [Fe(3,5-Me-BAFP)(NHOMe)] (**1**), as illustrated in Scheme 3. We further decided to use the sterically shielding bis-picket fence porphyrin H_2[3,5-Me-BAFP] as the ligand to stabilize the bound hydroxylamide group. The simplest reaction sequence to generate the target complex **1** would be the direct reaction of a ferric heme precursor with free NH_2OMe. However, previous work by our laboratory has shown that, although NH_2OR-type ligands are stable at room temperature, the reaction of free NH_2OR with iron(III) porphyrins still leads to disproportionation reactions.[28] We therefore speculated that akylhydroxylamide ($NHOR^-$) salts could be reacted with ferric [Fe(Porph)(X)] precursors (where $Porph^{2-}$ = dianion of a generic porphyrin coligand; X^- = weakly coordinating anion such as SbF_6^-, PF_6^-, ClO_4^-, etc.) under dry conditions to yield the desired Fe^{III}-NHOR porphyrin complexes, as an alternative synthetic route.

In order to test this idea, the hydroxylamide salt Li[NHOMe] was first prepared by direct deprotonation of NH_2OMe with methyllithium in dry diethyl ether at −80 °C, as previously reported.[26] The ferric hexafluorophosphate complex [Fe(3,5-Me-BAFP)(PF_6)], and related complexes with weakly coordinating counterions, were prepared as previously reported.[28] Then, excess Li[NHOMe] was reacted with the ferric [Fe(3,5-Me-BAFP)(X)] complexes in 2-Me-THF at room temperature to form the corresponding ferric methylhydroxylamide complex **1** in 81% yield. The UV−vis spectrum of the isolated product **1** (Figure 2) shows a broadening and a shift in the position of the Soret band from 401 to 422 nm, and a Q band shift from 525 to 582 nm. The UV−vis properties of **1** are indicative of an N-bound ferric reaction product such as [Fe(TPP)(4-MI)] (λ_{max} = 416, 576, and 621 nm in toluene; 4-MI = 4-methylimidazolate).[47] To determine whether the ferric hydroxylamide complex is high-spin (hs) or low-spin (ls), EPR spectroscopy was employed. The EPR spectrum of **1** in toluene at 6 K, shown in Figure 2, exhibits effective g values, $g_{eff,x} \approx g_{eff,y} \approx 5.94$, and $g_{eff,z} = 2.0$, which emanate from the "$M_s = \pm^1/_2$" doublet of the $S = {}^5/_2$

DOI: 10.1021/acs.inorgchem.8b02947
Inorg. Chem. XXXX, XXX, XXX−XXX

ground state with a rhombicity E/D of ≈0. In addition, the shifts of the β-pyrrole ^{1}H NMR signals of the porphyrin coligand are correlated with the oxidation and spin state of the iron center.[48−50] Our complex, **1**, exhibits a broad signal at ∼79 ppm in the ^{1}H NMR spectrum that is representative of a hs $S = {}^5/_2$ complex. The remaining porphyrin protons are found in the 11−1.8 ppm range. Interestingly, we also observed two broad signals from the bound NHOMe$^-$ ligand at −0.89 and −3.76 ppm, as shown in Figure S3. These signals are shifted upfield, respectively, because of the ring current of the porphyrin coligand.

To further confirm that the coordination of the methylhydroxylamide ligand in our Fe^{III}-NHOMe$^-$ complex is consistent with our expectation (see the proposed structure in Scheme 3), we obtained the crystal structure of this complex shown in Figure 3. In the structural model of **1**, the iron is

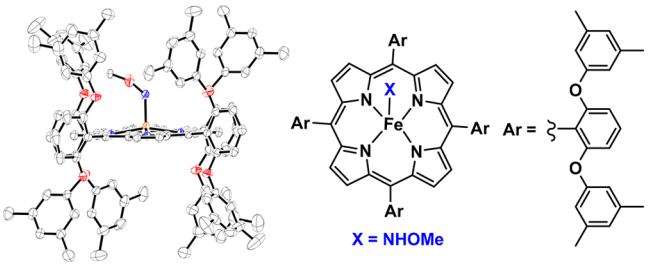

Figure 3. Left: Crystal structure of **1**. Hydrogen atoms and the disorder of the NHOMe$^-$ ligand are omitted for clarity. The thermal ellipsoids are shown at 30% probability. Right: Schematic drawing of **1**.

disordered above and below the heme plane and the methylhydroxylamide ligand bound to the iron center is also disordered. The hydroxlyamide ligand contains a 4-fold disorder of the NHOMe$^-$ group. Importantly, the structure shows that the NHOMe$^-$ ligand is bound through its nitrogen atom as anticipated. The fact that the iron center is located above the heme plane, toward the NHOMe$^-$ ligand, is a clear indication that the complex is indeed five-coordinate (5C). The average Fe−N$_{porph}$ bond length for our complex is 2.069 Å, which falls into the range of other hs (and 5C) ferric porphyrins (2.051−2.082 Å), as shown in Table 1.[51−53] Interestingly, the Fe−NHOMe bond length is 1.918 Å, which is most similar to the Fe−N$_3$ bond length in [Fe(TPP)(N$_3$)] of 1.953 Å.[51] However, our complex exhibits a longer Fe−NHOMe bond compared to the Fe−OMe bond length of 1.816 Å in [Fe(TPP)(OMe)],[52] whereas it is significantly shorter than the Fe−Cl bond (2.192 Å) in [Fe(TPP)(Cl)].[53] It is also worth noting that, because the iron sits above the heme plane, 5C ferric porphyrins usually show some degree of the doming distortion, which is typically analyzed by measuring the iron atom displacement from the mean heme plane (toward the axial ligand). In the crystal structure of **1**, the iron atom is displaced by 0.345 Å from the mean heme plane, which is within range (although on the lower end) of the reported iron atom displacements of 0.39−0.62 Å observed for 5C hs ferric porphyrin complexes.[54] This indicates that our complex is less domed compared to other 5C ferric heme complexes from the literature.

Last, we characterized complex **1** by ^{57}Fe NRVS to identify the Fe−N stretching mode of this compound. The NRVS data in Figure S4 (top) show noteworthy features at 250 and 558 cm^{-1}. The lower-energy band at 250 cm^{-1} represents the e$_u$-symmetric Fe−N(porphyrin) stretching vibration, the energy of which is representative of a hs ferric complex.[55−57] By comparison to the NRVS spectrum of the precursor complex [^{57}Fe(3,5-Me-BAFP)(SbF$_6$)], the 558 cm^{-1} band in **1** could correspond to the Fe−N stretch of the methylhydroxylamide ligand. To gain further insight into the vibrational assignments, we performed DFT calculations. The structure of [Fe(P)(NHOMe)] (where P^{2-} = porphine) was fully optimized with BP86/TZVP, and the vibrational frequencies were calculated. Overall, the optimized structure is in good agreement with our crystal structure data (Table 1). The calculated Fe−N bond length is 1.94 Å, while the crystal structure value is 1.918 Å. The calculated N−O bond length of the methylhydroxylamide ligand is 1.408 Å, whereas the crystal structure bond length is ∼0.1−0.2 Å longer (1.509−1.606 Å). The Fe−N−O bond angle of the crystal structure is 116−125°, which is consistent with the calculated bond angle of 125°.

Importantly, the calculated NRVS data show very good agreement with experiment (Figure S4) and predict the Fe−N stretching frequency of the methylhydroxylamide ligand at 565 cm^{-1}, which is very similar to the experimental band at 558 cm^{-1}, in terms of both the energy and intensity. We therefore assign this feature to the Fe−NHOMe stretch.

In summary, we have synthesized the first example of a 5C ferric hydroxylamide complex, **1**, in pure form and fully characterized the complex by UV−vis, EPR, and ^{1}H NMR spectroscopy, NRVS, and X-ray crystallography.

Electrochemistry of 1. The electrochemistry of complex **1** was studied by cyclic voltammetry (CV), in order to determine whether one-electron oxidation of this complex is possible. CV of the ferric methylhydroxylamide complex exhibits a chemically reversible one-electron oxidation at a reduction potential of +0.291 V vs Fc$^+$/Fc (in 1,2-dichloroethane), as shown in Figure 4, left. Interestingly, the one-electron oxidation product appears to be stable on the time scale for CV measurements.

Table 1. Comparison of the Geometric Parameters of Selected Iron Porphyrin Complexes to 1[a] and the Calculated Structure of This Complex with BP86/TZVP (Using P^{2-} = Porphine Dianion in the Calculations)

complex	ΔFe−N$_{porh}$[b]	ΔFe−L[c]	ΔO−C	ΔN−O	∠Fe−L	ref
[Fe(3,5-Me-BAFP)(NHOMe)] (**1**)	2.0695	1.918	1.487[d]	1.522[e]	125[f]	t.w.
[Fe(P)(NHOMe)], calculated	2.10	1.940	1.438	1.408	124	t.w.
[Fe(TPP)(N$_3$)]	2.066	1.953			122	48
[Fe(TPP)(OMe)]	2.082	1.816	1.393		129	49
[Fe(TPP)(Cl)]	2.051	2.192				50

[a]Bond lengths are given in Å and the angles in degrees. [b]Average value. [c]L denotes the axial ligand bound to the iron center. [d]The NHOMe$^-$ unit is disordered, resulting in additional C−O bond lengths of 1.434, 1.447, and 1.480 Å. [e]Additional N−O bond lengths = 1.509, 1.570, and 1.606 Å. [f]Additional ∠Fe−NH−OMe = 116, 119, and 124°.

DOI: 10.1021/acs.inorgchem.8b02947
Inorg. Chem. XXXX, XXX, XXX−XXX

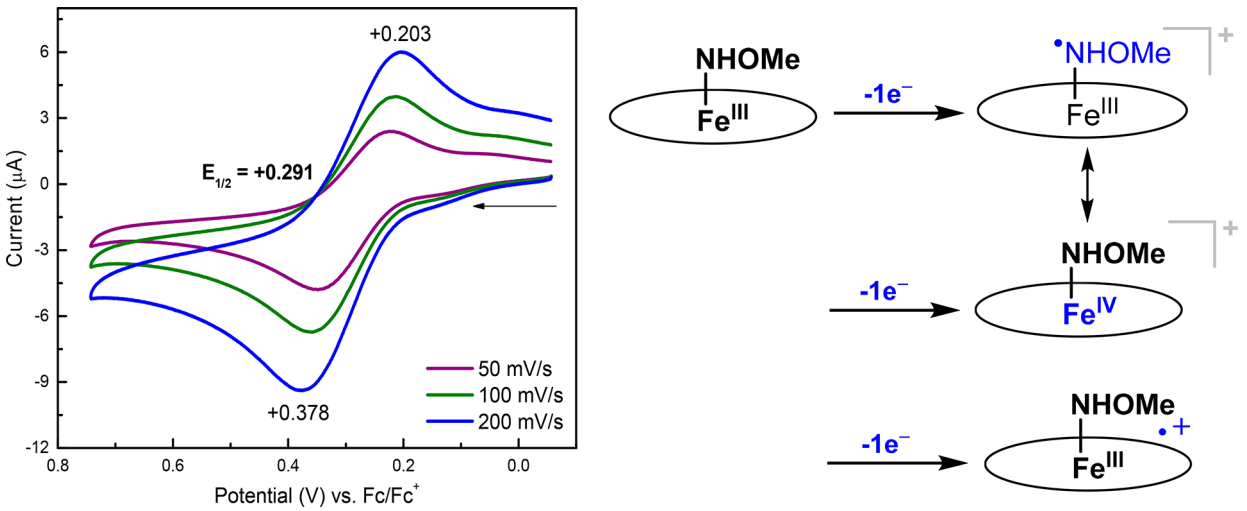

Figure 4. CV of a 3 mM solution of **1** in 1,2-dichloroethane that contained 0.10 M tetrabutylammonium hexafluorophosphate, using a glassy carbon working electrode, a platinum counter electrode, and a silver wire pseudoreference electrode at room temperature. Right: Schematic representation of the one-electron oxidation of **1**, which could result in oxidation of the Fe-NHOMe$^-$ unit or the porphyrin co-ligand. The oval represents the porphyrin ligand.

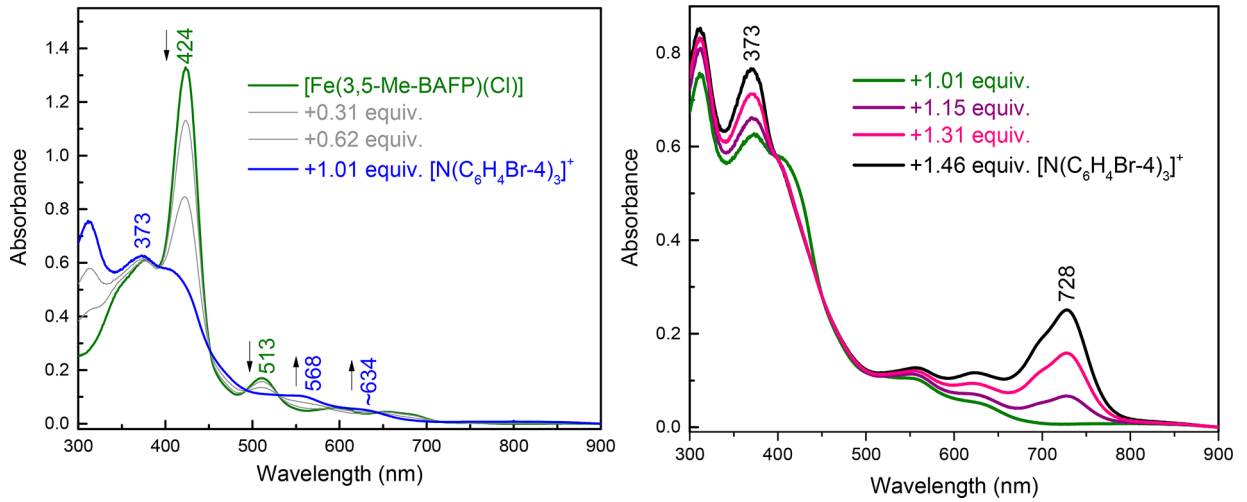

Figure 5. Left: UV−vis spectra of the titration of a ∼ 11 μM solution of [Fe(3,5-Me-BAFP)(Cl)] (green) with the chemical oxidant $[N(C_6H_4Br\text{-}4)_3][SbCl_6]$, in dichloromethane, to form the ferric porphyin radical complex $[Fe(3,5\text{-Me-BAFP})(Cl)]^+$ (blue). Right: UV−vis spectra obtained upon the addition of excess oxidant, showing that the reaction is complete after the addition of 1 equiv of oxidant. The bands at 373 and 728 nm are from the oxidant $[N(C_6H_4Br\text{-}4)_3][SbCl_6]$. The reactions were carried out at room temperature.

Complex **1** should exhibit a (formal) Fe^{III}/Fe^{IV} redox couple and two additional oxidations of the porphyrin macrocycle. The solvent window in 1,2-dichloroethane cuts off around +1 V, but we still observe another quasi-reversible redox event at ∼+0.90 V versus Fc^+/Fc.

On the basis of the CV data for complex **1** alone, it is not possible to say which group is actually oxidized at the first oxidative wave at +0.291 V. Figure 4, right, shows the three possibilities: the oxidation could either be metal-centered, transforming the complex from Fe^{III} to Fe^{IV}, it could be hydroxylamide-centered, creating a corresponding Fe^{III}-$(NHOMe)^•$ system, or the oxidation could occur on the porphyrin coligand. The latter process would not be biologically relevant (in terms of modeling Intermediate I), and, hence, it is important to clearly rule out this possibility. In order to do this, it would be most meaningful to study a closely related complex (with the same porphyrin ligand) that actually shows a porphyrin-ligand centered oxidation and, in this way, would allow us to determine the spectroscopic features associated with an oxidized 3,5-Me-$BAFP^{2-}$ porphyrin macrocycle.

Oxidation of [Fe(3,5-Me-BAFP)(Cl)]. It is reported in the literature that one-electron oxidation of ferric heme chloride complexes, [Fe(Porph)(Cl)], results in the oxidation of the porphyrin coligand to yield an Fe^{III}-$(porphyrin)^{•+}$ complex (rather than oxidation of the iron center to an Fe^{IV} species).[58−61] To gain a spectroscopic handle on porphyrin ring oxidation with our 3,5-Me-$BAFP^{2-}$ porphyrin ligand, we carried out one-electron oxidation of [Fe(3,5-Me-BAFP)(Cl)]. The cyclic voltammogram of [Fe(3,5-Me-BAFP)(Cl)] is shown in Figure S5, which exhibits the first reversible oxidation event at an $E_{1/2}$ value of +0.519 V versus Fc^+/Fc in 1,2-dichloroethane. Interestingly, this value is ∼200 mV more negative than the $E_{1/2}$ value of [Fe(TPP)(Cl)] at +0.73 V (vs Fc^+/Fc in CH_2Cl_2). The redox potential of our complex is actually closer to that of the complex [Fe(T*p*-OCH_3PP)(Cl)],

DOI: 10.1021/acs.inorgchem.8b02947
Inorg. Chem. XXXX, XXX, XXX−XXX

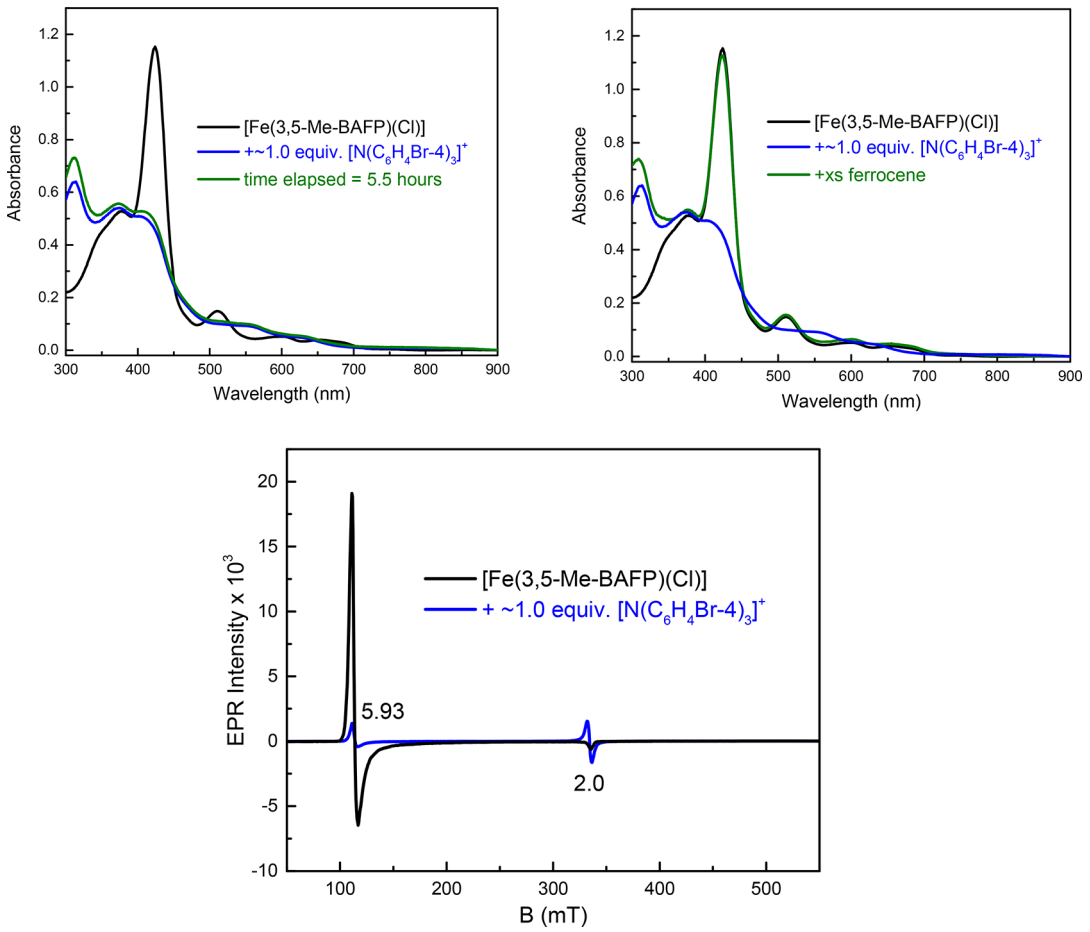

Figure 6. Top left: UV−vis spectra of [Fe(3,5-Me-BAFP)(Cl)] before (black) and after the addition of ∼1 equiv of $[N(C_6H_4Br\text{-}4)_3][SbCl_6]$ in dichloromethane (blue), leading to formation of the ferric porphyrin radical complex $[Fe(3,5\text{-}Me\text{-}BAFP)(Cl)]^+$. The reaction product after stirring for 5.5 h under an inert atmosphere at room temperature is shown in green. Top right: Subsequent reaction of the oxidized species with excess ferrocene that re-forms the [Fe(3,5-Me-BAFP)(Cl)] complex (green). Bottom: EPR spectra of a 1.2 mM solution of the ferric chloride complex [Fe(3,5-Me-BAFP)(Cl)] and of the reaction product upon the addition of ∼1 equiv of $[N(C_6H_4Br\text{-}4)_3][SbCl_6]$, measured at 5 K in dichloromethane.

which contains the tetraphenylporphyrin derivative T*p*-OCH_3PP [dianion of tetra(*p*-methoxyphenyl)porphyrin]. This complex shows an $E_{1/2}$ value of +0.64 V (vs Fc^+/Fc in CH_2Cl_2).[60]

Next, we employed UV−vis spectroelectrochemistry (SEC) to determine whether or not the oxidized complex $[Fe(3,5\text{-}Me\text{-}BAFP)(Cl)]^+$ contains a porphyrin radical ligand. Oxidation of a solution of [Fe(3,5-BAFP)(Cl)] (Figure S6) results in a significant decrease in the intensity of the Soret band at 425 nm, while the Cl^--to-Fe charge-transfer feature at 373 nm remains relatively unchanged.[62] This results in a broad, split Soret band. At the same time, the main Q band at 513 nm decreases in intensity as two new bands grow in at 568 and 634 nm. The oxidation is completely reversible, as shown in Figure S6. In comparison to the results for the analogous complex [Fe(TPP)(Cl)], these changes in the absorption spectrum are indeed characteristic for porphyrin ring oxidation and, in this case, formation of an Fe^{III}-$(porphyrin)^{\bullet+}$ complex.[58−60]

Using a chemical oxidant, we were also able to generate the oxidized complex $[Fe(3,5\text{-}Me\text{-}BAFP)(Cl)]^+$ in bulk at room temperature for further spectroscopic studies. For this purpose, the ferric chloride precursor complex [Fe(3,5-Me-BAFP)(Cl)] was titrated with a solution of the oxidant tris(4-bromophenyl)ammoniumyl hexachloroantimonate, $[N(C_6H_4Br\text{-}4)_3][SbCl_6]$ ($E_{1/2}$ = +0.70 V vs Fc^+/Fc in CH_2Cl_2).[61] The reaction is complete upon the addition of ∼1 equiv of $[N(C_6H_4Br\text{-}4)_3][SbCl_6]$, as shown in Figure 5, left. The addition of more than 1 equiv of oxidant simply results in an increase in the absorption bands of the oxidant itself at 373 and 728 nm (Figure 5, right). The UV−vis spectrum of the reaction product from chemical oxidation is essentially identical with that of the UV−vis SEC-generated species (Figure S6). In addition, Figure 6 shows that chemical oxidation is completely reversible upon the addition of excess ferrocene to the oxidized species $[Fe(3,5\text{-}Me\text{-}BAFP)(Cl)]^+$. To further access the purity of the bulk material, we utilized EPR and ^1H NMR spectroscopy. For these experiments, the ferric chloride precursor was dissolved in dichloromethane (1−2 mM) and added to excess solid oxidant, $[N(C_6H_4Br\text{-}4)_3][SbCl_6]$, and the solution was then agitated until all of the solid had dissolved. The progress of the reaction was monitored by UV−vis spectroscopy. The EPR spectrum at 5 K of the ferric chloride precursor has a hs ferric signal with $g_{eff,x} \approx g_{eff,y} \approx 5.93$ and $g_{eff,z} = 2.0$, corresponding to the ground-state Kramers doublet of $S = {}^5/_2$ with E/D of ≈0. The addition of ∼1.0 equiv of oxidant to the solution of the ferric chloride complex results in a completely EPR-silent species, shown in Figure 6, bottom. This indicates that a clean conversion to the

DOI: 10.1021/acs.inorgchem.8b02947
Inorg. Chem. XXXX, XXX, XXX−XXX

oxidized species [Fe(3,5-Me-BAFP)(Cl)]$^+$ has taken place. Next, we used ^{1}H NMR spectroscopy to determine the spin state of the iron center in the oxidized porphyrin complex. As previously mentioned, the β-pyrrole hydrogen atoms of the porphyrin coligand shift as a function of the iron oxidation and spin state. For the ferric chloride precursor (hs, $S = {}^5/_2$), the chemical shifts range from 2 to 80 ppm and are paramagnetically broadened in deuterated dichloromethane. The broad peak at ~80 ppm corresponds to the β-pyrrole hydrogen atoms of the porphyrin coligand (Figure S7, top), which is indicative of a hs ferric heme complex. The addition of excess [N(C_6H_4Br-4)$_3$][$SbCl_6$] to the ferric chloride complex results in a ^{1}H NMR spectrum with chemical shifts that range from 80 to −11 ppm and that are still paramagnetically broadened, as shown in Figure S7, bottom. The upfield shift of some of the porphyrin peaks is indicative of oxidation of the porphyrin macrocycle.[63,64] Analogous to the ferric chloride precursor, the β-pyrrole hydrogen atoms are observed as a broad peak at ~83 ppm. This demonstrates that [Fe(3,5-Me-BAFP)(Cl)]$^+$ is a hs ferric complex with an oxidized porphyrin macrocycle. It should be noted that the electronic structure of [Fe(TPP)(Cl)]$^+$ has been studied in detail with techniques probing the magnetic properties such as NMR magnetic susceptibility, SQUID magnetization, and Mössbauer spectroscopy to confirm the quintet ($S = 2$) ground state of this complex.[58,60,64,65] On the basis of these results, we can further conclude that the electronic structure of the oxidized complex [Fe(3,5-Me-BAFP)(Cl)]$^+$ is best described as a hs ferric complex ($S = {}^5/_2$) that is antiferromagnetically coupled to the porphyrin radical coligand ($S = {}^1/_2$), resulting in a total spin of $S = 2$. In summary, we generated the ferric porphyrin radical complex [Fe(3,5-Me-BAFP)(Cl)]$^+$ in pure form and characterized this complex by UV−vis, EPR, and ^{1}H NMR spectroscopy, which provides an important benchmark in terms of identifying the location of the oxidation in complex **1**.

Formation of a Model Complex for Intermediate I. First, the chemical oxidant [DAcFc][SbF_6] was synthesized by the reaction of 1,1′-diacetylferrocene with [thianthrene]-[SbF_6][66] in dichloromethane, as previously reported by our laboratory.[30] For the following chemical oxidation studies, the oxidant was dissolved in cold DME because of its poor solubility (<1 mM) in the solvents toluene and dichloromethane, used to dissolve the iron porphyrin methylhydroxylamide complex.

Then, the reaction of the Fe^{III}-$NHOMe^-$ complex with 1 equiv of the chemical oxidant [DAcFc][SbF_6] was monitored in situ in toluene at room temperature using UV−vis spectroscopy under an inert atmosphere (in the glovebox). The reaction product generated in this way exhibits a Soret band at 409 nm and the main Q band at 525 nm (Figure S8, left). This spectrum is nearly identical to that of [Fe(3,5-Me-BAFP)(SbF_6)] (Figure S8, right). The EPR spectrum of the reaction product also matches that of [Fe(3,5-Me-BAFP)-(SbF_6)], with an additional, minor signal from another rhombic iron species, as shown in Figure S9. One possible route to form [Fe(3,5-Me-BAFP)(SbF_6)] from the oxidation of **1** would be by dissociation of the putative (NHOME)$^\bullet$ ligand from the metal center, as shown in Scheme 4. On the basis of previous reports in the literature, the free (NHOME)$^\bullet$ molecule dimerizes to form a hyponitrite-like compound, $N_2O_2Me_2$, which, however, does not produce N_2O upon decomposition but dinitrogen and methanol.[67−69] Because of rapid decomposition of the oxidized complex [Fe(3,5-Me-BAFP)(NHOMe)]$^+$ (**1**$^+$) at room temperature, we then conducted the oxidation of **1** at −80 °C under an inert atmosphere and monitored the reaction by in situ UV−vis spectroscopy via a low-temperature immersion probe.

Scheme 4. Chemical Oxidation of 1 and Subsequent Decomposition of the Oxidized Species To Yield [Fe(3,5-Me-BAFP)(SbF_6)]

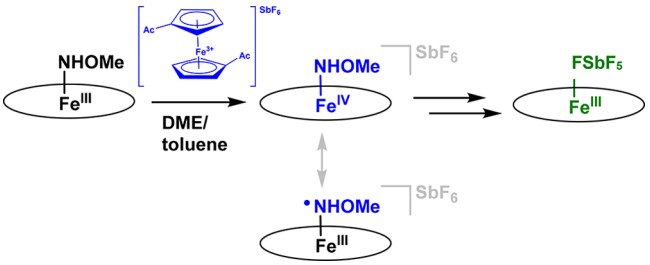

The addition of ~1 equiv of the oxidant [DAcFc][SbF_6] to a solution of the ferric hydroxlyamide complex in toluene at −80 °C results in a small decrease in the intensity of the Soret band at 424 nm, along with shifts in the Q-band region from 582 and 626 nm to 570 and 617 nm, respectively, as shown in Figure 7. Importantly, the UV−vis spectrum of the low-temperature product is different compared to the room temperature product [Fe(3,5-Me-BAFP)(SbF_6)] (λ_{max} = 409 and 525 nm; Figure S8). Also, the UV−vis spectrum of **1**$^+$ does not exhibit features associated with the formation of a porphyrin radical (porphyrin ligand oxidation), as would be evident from a breakdown of the Soret band, as observed for [Fe(3,5-Me-BAFP)(Cl)]$^+$ (see above). Excitingly, this directly indicates that it is, in fact, the Fe^{III}-$NHOMe^-$ unit that is oxidized in **1**$^+$. We also monitored (by UV−vis) the stability of the oxidized complex at −80 °C. Over a 1 h time period, the Q band at 570 nm slowly decreases in intensity, while a new band grows in at 525 nm (Figure S10, left). The decay of the Q band at 570 nm plotted versus time can be fit to a single exponential (Figure S10, right) with $k_{obs} = 1.7 \times 10^{-4}$ s^{-1} and a half-life of ~68 min. This means that the oxidized species **1**$^+$ is mostly decomposed within a 3 h time period at −80 °C. When the solution of the oxidized species is warmed up to room temperature, it is found that this species rapidly decomposes (in ~10 min) to yield [Fe(3,5-Me-BAFP)(SbF_6)], which is the same product that is obtained when the reaction is conducted at room temperature. Interestingly, Intermediate I in P450nor also decays into a ferric complex upon decomposition.[24] Although the oxidized species **1**$^+$ is quite *unstable*, our work shows that there is a modest time window at −80 °C to obtain samples for further spectroscopic characterization and conduct reactivity studies with this compound. To determine the purity of the oxidized complex **1**$^+$, EPR spectroscopy was employed. The Fe^{III}-$NHOMe^-$ precursor is EPR-active with an $S = {}^5/_2$ ground state as mentioned above. Upon oxidation, the complex becomes integer-spin (S = 1 or 2) and EPR-silent. The EPR spectra in Figure S11 show that the oxidized complex **1**$^+$ can be obtained with ~85% purity, which is suitable for the conduction of further reactivity studies. The purity was determined from integral EPR intensities using the program *SpinCount*.

Electronic Structure of 1$^+$. As mentioned in the Introduction, one remaining key question with respect to the mechanism of P450nor is the exact electronic structure of Intermediate I. In order to gain insight into this issue, we used

DOI: 10.1021/acs.inorgchem.8b02947
Inorg. Chem. XXXX, XXX, XXX−XXX

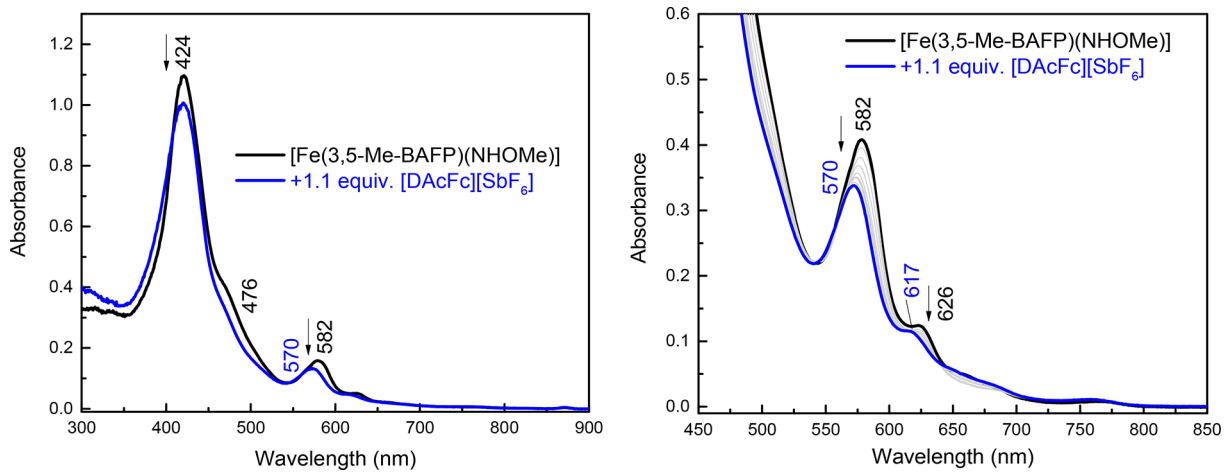

Figure 7. Left: UV−vis spectra monitoring the reaction of a ∼6 μM solution of **1** (black) with 1.1 equiv of [DAcFc][SbF_6] in toluene (blue). Right: UV−vis spectra following the reaction of a ∼38 μM solution of **1** (black) with 1.1 equiv of [DAcFc][SbF_6] in toluene (blue). All reactions were carried out under an inert atmosphere at −80 °C.

different spectroscopic methods to investigate the electronic structure of our model system for Intermediate I, $\mathbf{1}^+$. After having ruled out oxidation of the porphyrin ring in model system $\mathbf{1}^+$ (and this can also be ruled out for Intermediate I, based on the optical data),[11,70] we are left with two possible valence tautomers: complex $\mathbf{1}^+$ can be described as either an Fe^{IV}-$NHOMe^-$ or an Fe^{III}-$(NHOMe)^\bullet$ complex (Scheme 1). In order to gain insight into the electronic structure of $\mathbf{1}^+$, we first applied rRaman spectroscopy. It has previously been established that some of the core vibrations of the porphyrin coligand in the 1300−1650 cm^{-1} range are sensitive to the oxidation and spin state of the iron center.[71−73] For example, the symmetric $C-N_{pyrrole}$ stretching vibration constitutes the oxidation-state marker band (ν_4).[74] This mode usually ranges from 1340 to 1375 cm^{-1}, depending on the iron oxidation state.[75] The rRaman spectrum of the ferric precursor **1** in toluene at 77 K (Figure 8) shows the ν_4 band at 1364 cm^{-1}, which is typical for a ferric complex. Excitingly, this mode is observed at the same frequency (1364 cm^{-1}; Figure 8) in the spectrum of the oxidized complex $\mathbf{1}^+$ (formed with ∼1 equiv of [DAcFc][SbF_6]), which clearly indicates that the iron center is still in the Fe^{III} oxidation state. As a further control, we warmed the solution of the oxidized complex $\mathbf{1}^+$ to room temperature and measured the rRaman spectrum of the resulting species, which we believe is [Fe(3,5-Me-BAFP)(SbF_6)] based on the UV−vis results discussed above. This sample shows a split oxidation state marker band at 1347 and 1364 cm^{-1}. The splitting in the oxidation state marker band is a characteristic feature of ferric heme complexes with a spin-admixed ($S = {}^3/_2$ and ${}^5/_2$) ground state.[76,77] To further confirm this finding, the rRaman spectrum of an independently prepared sample of [Fe(3,5-Me-BAFP)(SbF_6)] was measured in a frozen toluene/DME solution, which leads to a very similar spectrum compared to that of the decomposed product (Figure S2). From these data, we hypothesize that the oxidized species is a ferric complex with a bound $(NHOMe)^\bullet$ ligand rather than an iron(IV) species.

In addition, the spin-state marker band (ν_2), which is typically observed in the 1535−1570 cm^{-1} range, can be consulted to obtain information about the spin state of the complex.[75] In the Fe^{III}-$NHOMe^-$ precursor, three bands are observed at 1548, 1562, and 1573 cm^{-1} (Figure 8; not

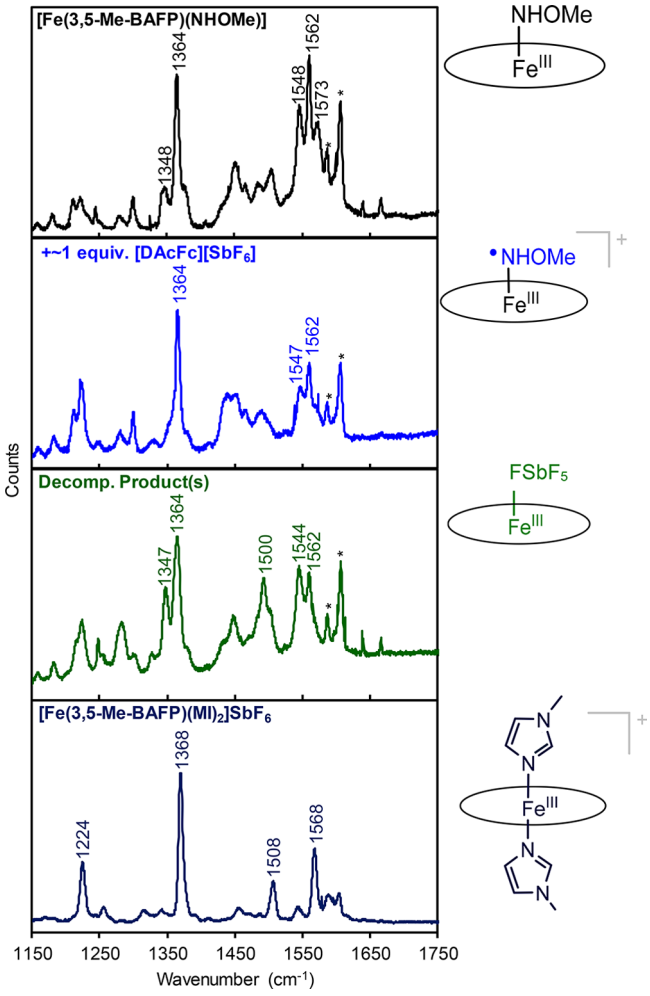

Figure 8. rRaman spectra of frozen solutions of ∼0.26 mM **1** (black), the reaction product upon the addition of ∼1 equiv of [DAcFc]-[SbF_6] (blue), the reaction product(s) after the solution is warmed up to room temperature (green), and a 0.60 mM solution of a ls ferric complex, [Fe(3,5-Me-BAFP)$(MI)_2$]SbF_6 (dark blue; MI = 1-methylimidazole) in a 5:1 ratio of toluene/DME [laser power = 28 mW for all complexes, except the MI-bound complex (laser power = 17 mW)]. The asterisks denote bands from toluene.

DOI: 10.1021/acs.inorgchem.8b02947
Inorg. Chem. XXXX, XXX, XXX−XXX

observed in the toluene/DME blank shown in Figure S21), with the 1562 cm^{-1} band being the most intense. For comparison, in the hs complex [Fe(3,5-Me-BAFP)(Cl)], there is a single band at 1560 cm^{-1} (Figure S19, top). We propose that the splitting of the 1560 cm^{-1} feature into three bands in **1** is likely due to the presence of rotational isomers of the Fe-NHOMe group. In the oxidized complex $\mathbf{1}^+$, the 1573 cm^{-1} band disappears, while the two bands at 1547 and 1562 cm^{-1} remain, with the 1562 cm^{-1} feature still being the most intense. For comparison to a ls complex with this porphyrin coligand, we prepared a solution of the ferric bis(imidazole) complex $[Fe(3,5\text{-Me-BAFP})(MI)_2]SbF_6$ (MI = 1-methylimdazole). In this complex, the ν_2 band is shifted to 1568 cm^{-1} (Figure 8). This indicates that the oxidized complex $\mathbf{1}^+$ is, in fact, a hs ferric species.

Along with rRaman studies, Mössbauer spectroscopy was employed to investigate the electronic structure of the oxidized species $\mathbf{1}^+$. The precursor **1** exhibits a magnetically split Mössbauer spectrum and can be fit with parameters typical of hs iron(III) heme centers: δ = 0.50 mm/s, ΔE_Q= −0.41 mm/s, asymmetry parameter η = 0.2, and ^{57}Fe hyperfine tensor $\mathbf{A}/g_n\beta_n$ = (−20, −20, −20) T (Figure 9). The addition of oxidant

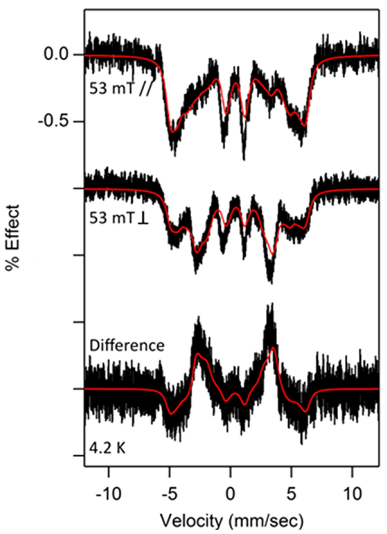

Figure 9. 4.2 K/53 mT Mössbauer spectra of a ∼2 mM solution of **1** frozen in a 5:1 ratio of toluene/DME, where the γ beam was applied parallel (top) or perpendicular (middle) to the applied magnetic field, and the corresponding parallel-minus-perpendicular difference spectrum (bottom). Experimental data and simulations are shown as black bars and red lines, respectively. Simulations were carried out in the slow relaxation limit with the following parameters: $S = {}^5/_2$, g_{iso} = 2.0, D = 3 cm^{-1}; E/D = 0.05; ΔE_Q = −0.41 mm/s; δ = 0.50 mm/s; η = 0.2; $\mathbf{A}/g_n\beta_n$ = (−20.0, −20.0, −20.0) T.

to **1** results in a Mössbauer spectrum that shows a quadrupole doublet with δ = 0.43 mm/s and $|\Delta E_Q|$ = 0.75 mm/s (Figure 10). The isomer shift is altered only slightly from that of the precursor, which suggests that the oxidized complex is still a hs ferric species. Also, the isomer shift values are in good agreement with other hs ferric complexes, where δ usually ranges from 0.35 to 0.45 mm/s. In contrast, iron(IV) heme species have isomer shifts in the range $\delta \approx 0$−0.15 mm/s.[78−83]

In summary, rRaman and Mössbauer spectroscopies provide insight into the oxidation and spin state of our model complex $\mathbf{1}^+$ and show clearly that this species is best described as the hs Fe^{III}-$(NHOMe)^\bullet$ valence tautomer.

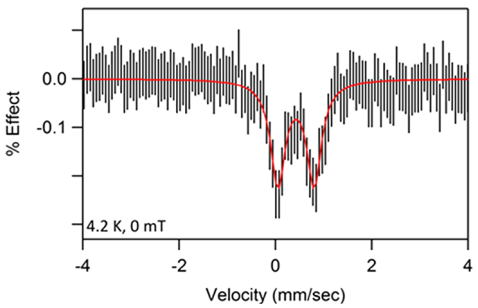

Figure 10. 4.2 K Mössbauer spectrum of a ∼0.3 mM solution of $\mathbf{1}^+$ frozen in a 5:1 ratio of toluene/DME in the absence of a magnetic field (black bars), with the quadrupole doublet simulation shown as a red line. Simulation parameters used are given as follows: δ = 0.43 mm/s; $|\Delta E_Q|$ = 0.75 mm/s.

Reactivity of $\mathbf{1}^+$ with NO. Finally, we studied the reactivity of the oxidized species $\mathbf{1}^+$ with NO to determine if an intermediate of this type would be catalytically competent in P450nor catalysis. First, using in situ UV−vis spectroscopy, we monitored the reaction of the oxidized species at −80 °C with low equivalents of NO gas. This resulted in facile formation (total reaction time = ∼35 s at −80 °C) of a species with a 525 nm Q band, indicative of the formation of [Fe(3,5-Me-BAFP)(SbF_6)] (Figure 11, left). A single-exponential fit of these data delivers k_{obs} = 5 × 10^{-2} s^{-1} (Figure S13). After ∼110 s at −80 °C, the solution turns bright red along with a shift in the Q band from 525 to 542 nm, along with a new small shoulder at 577 nm (Figure 11, right). The energy and shape of the new bands are characteristic of a 6C ferric heme nitrosyl complex.[30] Further, the 6C ferric NO complex with the 3,5-Me-$BAFP^{2-}$ coligand, [Fe(3,5-Me-BAFP)(NO)(MI)]-SbF_6 (MI = 1-methylimidazole), shown in Figure S14 exhibits similar features (λ_{max} = 435, 546, and 585). Overall, these data suggest that $[Fe(3,5\text{-Me-BAFP})(NO)(L)]^+$ is formed due to excess NO in the solution, which binds to the initial product, [Fe(3,5-Me-BAFP)(SbF_6)], at −80 °C. We speculate that "L" is likely a solvent molecule such as DME that is present in excess relative to the iron porphyrin complex or a product from reaction of the oxidized complex $\mathbf{1}^+$ with NO gas. The rRaman spectrum of this subsequently formed NO product, $[Fe(3,5\text{-Me-BAFP})(NO)(L)]^+$, is shown in Figure S15. In this spectrum, the oxidation-state ν_4 marker band is shifted to 1369 cm^{-1} and the spin-state ν_2 marker band exhibits a split feature at 1560 and 1566 cm^{-1}. The 1369 and 1566 cm^{-1} features are consistent with other ferric heme-NO complexes,[28] which indicates that the heme is in a ls ferrous state (because these complexes have Fe^{II}-NO^+-type electronic structures). The split ν_2 maker band may suggest heme distortion in solution or the presence of a small amount of a ferric complex. This reaction sequence is summarized in Scheme 5.

Observation of the direct formation of [Fe(3,5-Me-BAFP)-(SbF_6)] from the reaction of $\mathbf{1}^+$ with NO without the formation of any intermediate iron nitrosyl species provides strong evidence for the direct attack of NO at the bound $(NHOMe)^\bullet$ ligand. Both the simple displacement of the $(NHOMe)^\bullet$ ligand by NO or the binding of NO to the open coordination site at the iron center would generate an $\{FeNO\}^6$ complex of the type $[Fe(3,5\text{-Me-BAFP})(NO)(L)]^+$ as the first intermediate of the reaction. Because these complexes are quite stable at −80 °C, they would be easily observed by UV−vis spectroscopy. In fact, we do observe NO

DOI: 10.1021/acs.inorgchem.8b02947
Inorg. Chem. XXXX, XXX, XXX−XXX

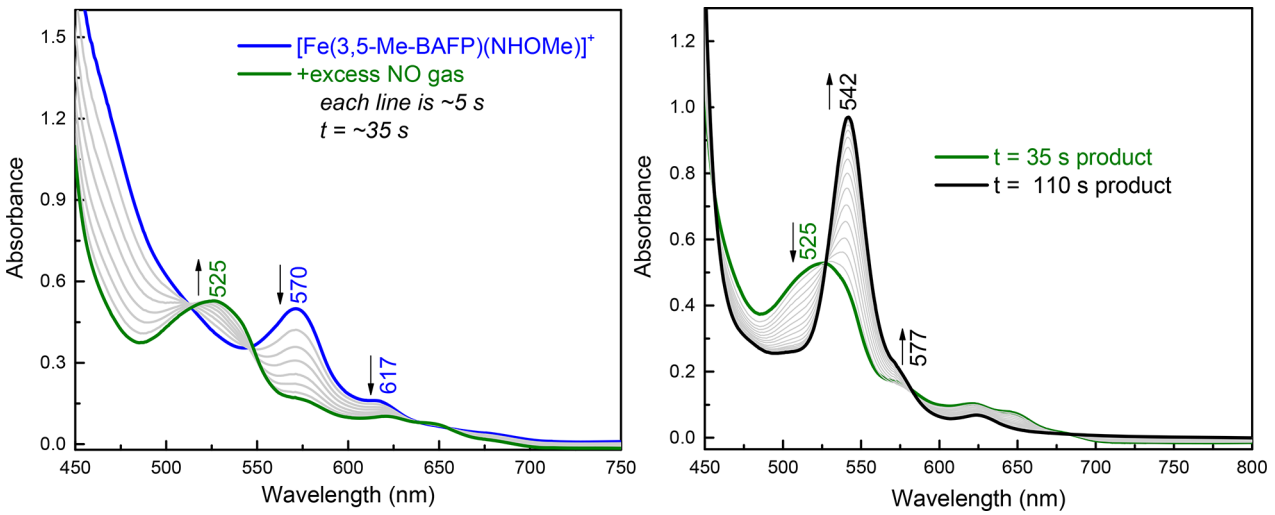

Figure 11. Left: In situ UV−vis monitoring of the reaction of $\mathbf{1}^+$ (blue) with excess NO gas at −80 °C. The final spectrum in green is identical to that of [Fe(3,5-Me-BAFP)(SbF_6)]. The precursor **1** was 46 μM, and 1.2 equiv of [DAcFc][SbF_6] and 2 mL of NO gas were used in this experiment. Right: Further reaction of the initial product with NO gas leads to the formation of a 6C ferric heme nitrosyl complex, [Fe(3,5-Me-BAFP)(NO)(L)]$^+$, where L is a neutral ligand. The intensity of the Soret band (<450 nm) is outside the range of the detector and, therefore, this feature is not included in the figures.

Scheme 5. Proposed Reaction Mechanism of the Reaction of [Fe(3,5-Me-BAFP)(NHOMe)]SbF_6 with Low Equivalents of NO Gas at −80 °C[a]

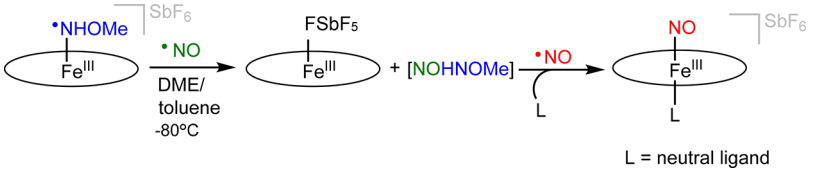

[a]L denotes a solvent molecule such as DME and/or a product from the reaction of [Fe(3,5-Me-BAFP)(NHOMe)]SbF_6 with NO gas.

binding to the initial product [Fe(3,5-Me-BAFP)(SbF_6)], which is due to the presence of excess NO, but this process is slower and happens on the minute time scale compared to the initial reaction of NO with $\mathbf{1}^+$, which happened on the second time scale. Nevertheless, this follow-up reaction further provides us with an authentic sample of the [Fe(3,5-Me-BAFP)(NO)(L)]$^+$-type species, allowing us to cleanly rule out the formation of an {FeNO}^{6} complex as the initial reaction product. We therefore propose that the first step of the reaction between $\mathbf{1}^+$ and NO corresponds to the fast attack of NO at the bound (NHOMe)$^\bullet$, which would correspond to a radical−radical coupling reaction that leads to N−N bond formation. These types of reactions are usually barrierless, which would explain why the reaction happens so fast, even at −80 °C. Correspondingly, the observed rate of reaction is likely only limited by the diffusion of NO gas into the solution.

When exactly 1 equiv of NO is used in the reaction with $\mathbf{1}^+$ [which requires a saturated solution of NO in CH_2Cl_2, where the NO concentration has been quantified with Co(TPP)], then $\mathbf{1}^+$ is fully converted to [Fe(3,5-Me-BAFP)(SbF_6)], indicating a 1:1 stoichiometry for the initial reaction. The rRaman spectrum of this product is shown in Figure S15, top. The ν_4 marker band is found at 1364 cm^{-1} and the spin-state ν_2 marker band exhibits a split feature at 1550 and 1557 cm^{-1}. This spectrum is noticeably distinct from the spectrum of [Fe(3,5-Me-BAFP)(NO)(L)]$^+$ (Figure S15, bottom). The data again show that the iron-based product in the initial reaction is [Fe(3,5-Me-BAFP)(SbF_6)], which demonstrates direct NO attack at the bound (NHOMe)$^\bullet$ ligand in $\mathbf{1}^+$.

Finally, we conducted further experiments to determine whether the reaction of $\mathbf{1}^+$ with NO could lead to porphyrin modification. For this purpose, the reaction mixture (after NO addition to $\mathbf{1}^+$) was shaken with ∼1 M hydrochloric acid, and the ferric chloro complex was then reisolated. The UV−vis spectrum of the product closely resembles an authentic sample of [Fe(3,5-Me-BAFP)(Cl)], shown in Figure S17. Both ^{1}H NMR and rRaman spectroscopy on this compound did not detect any porphyrin modification (Figures S18 and S19). The high-performance liquid chromatography/mass spectrometry data of this complex also showed the typical [M − Cl]$^+$ mass peak with no obvious changes in mass or alterations of the fragmentation pattern, as shown in Figure S20.

On the basis of all of these observations, we propose that the reaction of $\mathbf{1}^+$ with NO leads to fast N−N bond formation and generation of a hyponitrous acid analogue, HON-NOMe, which would be similar to the proposed reaction of Intermediate I with NO in P450nor catalysis. However, whereas hyponitrous acid (HON-NOH) itself is known to decompose into N_2O and water, the same cannot be expected for our product, HON-NOMe. There is no further information available in the literature with respect to the properties of such a species, but as mentioned above, it is known that MeON-NOMe decomposes into N_2 and methanol, and we would expect that HON-NOMe would follow a similar path. Nevertheless, we performed an IR gas headspace analysis[84]

DOI: 10.1021/acs.inorgchem.8b02947
Inorg. Chem. XXXX, XXX, XXX−XXX

after the reaction of $\mathbf{1}^+$ with NO, but to no surprise, we were not able to detect any N_2O (Figure S12). In a similar way, we also ruled out NO_2 as a reaction product. Other attempts to detect the product by NMR spectroscopy were also unsuccessful.

SUMMARY AND CONCLUSIONS

This work started off with the challenge of how to develop a model system for the critical Intermediate I of the P450nor reaction cycle. One possible way to accomplish this would be to follow the enzymatic reaction pathway, i.e., first generate a $\{FeNO\}^6$ complex and then react this species with a hydride donor, followed by protonation of the resulting HNO complex. Recent work in the literature has shown that this direct hydride transfer is indeed possible,[85,86] but these reactions (in the absence of a protein matrix) only deliver small amounts of the desired Fe^{II}-NHO complex. At the same time, large amounts of side products are formed because of hydride attack on the iron center and general decomposition. So, in summary, this pathway does not seem to be feasible for the preparation of a clean sample of an Intermediate I model complex. We therefore developed an alternative approach that completely circumvents all of these difficulties. Here, we first prepare a stable, ferric hydroxylamide complex and then simply oxidize this species by one electron to directly obtain a model system for Intermediate I. In this work, we used an O-alkylated hydroxylamine derivative, which provides stabilization to the ferric hydroxylamide complex and further directs the nitrogen atom of this ligand toward the iron center.

We first prepared the corresponding complex [Fe(3,5-Me-BAFP)(NHOMe)] (**1**) and characterized this species using different spectroscopic methods and X-ray crystallography. Our data show an N-coordinated $NHOMe^-$ ligand, as desired, with a relatively strong Fe−$NHOMe^-$ bond, as is evident from the corresponding Fe−NHOMe stretching frequency of 558 cm^{-1}, determined by NRVS. This complex shows a chemically reversible one-electron oxidation by CV, indicating that a stable model system for Intermediate I might be accessible with this compound. Indeed, chemical oxidation of **1** at −80 °C cleanly generates the corresponding, oxidized complex $[Fe(3,5\text{-Me-BAFP})(NHOMe)]^+$ ($\mathbf{1}^+$), which is the first model complex for Intermediate I reported to date. Comparison of the spectroscopic data for this complex to those of $[Fe(3,5\text{-Me-BAFP})(Cl)]^+$ rules our porphyrin ring oxidation and shows that it is indeed the Fe^{III}-$NHOMe^-$ unit that is oxidized in $\mathbf{1}^+$. Further rRaman and Mössbauer studies confirm this result and show that the oxidized complex is best described as an Fe^{III}-$(NHOMe)^\bullet$ species, which supports previous DFT results for Intermediate I in P450nor, where a similar electronic structure was proposed.[21] Excitingly, this species is competent for the reaction with NO, which proceeds within 30 s even at −80 °C. Because the NHOMe ligand is bound as a radical in $\mathbf{1}^+$, we propose that the reaction with NO corresponds to a barrierless radical−radical-type coupling reaction that leads to fast and efficient N−N bond formation. Importantly, no iron nitrosyl complex is formed in the initial stage of this reaction (or not at all if only 1 equiv of NO is added), which emphasizes the direct attack of NO at the $(NHOMe)^\bullet$ ligand, leading to the formation of $[Fe(3,5\text{-Me-BAFP})(SbF_6)]$.

These results provide direct evidence that if Intermediate I should indeed correspond to the doubly protonated Fe-NHOH complex, this species is likely of the Fe^{III}-$(NHOH)^\bullet$ type, as our studies have shown that this is the preferred electronic structure of such a species. Our results therefore directly support the previous DFT results. In addition, our work indicates that this type of intermediate is ideally suited to undergo fast N−N bond formation in a radical−radical-type coupling scenario by direct NO attack at the bound $(NHOH)^\bullet$ ligand. This radical is so reactive that is scavenges NO before it can even coordinate to the iron center (in the case of our model complex). Our new model complex, $\mathbf{1}^+$, therefore provides key insight into the electronic structure and reactivity of the key Intermediate I in P450nor catalysis. Of course, complex $\mathbf{1}^+$ is not a perfect model for Intermediate I because it is only a 5C species, whereas in the enzyme, this species would be 6C with a proximal thiolate (cysteinate) ligand bound. In order to further refine our results, we therefore attempted to coordinate an axial imidazole ligand to complex $\mathbf{1}^+$. Preliminary data indicate that this leads to the formation of a corresponding 6C complex, which is accompanied by a spin-state change from hs to ls. However, this also leads to a dramatic destabilization of the $(NHOMe)^\bullet$ intermediate and a drop in its half-life from ∼1 h to only 10−15 min, which makes it very difficult to work with this complex. Future studies are now aimed at finding ways to increase the stability of the 6C species, for further spectroscopic and reactivity studies.

ASSOCIATED CONTENT

Supporting Information

The Supporting Information is available free of charge on the ACS Publications website at DOI: 10.1021/acs.inorgchem.8b02947.

UV−vis, NMR, rRaman, EPR, and FT-IR spectra and crystallographic information for **1** (PDF)

Accession Codes

CCDC 1872862 contains the supplementary crystallographic data for this paper. These data can be obtained free of charge via www.ccdc.cam.ac.uk/data_request/cif, or by emailing data_request@ccdc.cam.ac.uk, or by contacting The Cambridge Crystallographic Data Centre, 12 Union Road, Cambridge CB2 1EZ, UK; fax: +44 1223 336033.

AUTHOR INFORMATION

Corresponding Author

*E-mail: lehnertn@umich.edu.

ORCID

Carsten Krebs: 0000-0002-3302-7053

Nicolai Lehnert: 0000-0002-5221-5498

Notes

The authors declare no competing financial interest.

ACKNOWLEDGMENTS

This work was supported by a grant from the National Science Foundation (Grant CHE-1464696 to N.L.). A.B.M. acknowledges a Rackham Merit Fellowship and a Wayne & Carol Pletcher Graduate Research Fellowship (University of Michigan). We acknowledge funding from NSF Grant CHE-0840456 for X-ray instrumentation. This research used resources of the APS, a U.S. Department of Energy (DOE) Office of Science User Facility operated for the U.S. DOE Office of Science by ANL under Contract DE-AC02-06CH11357.

DOI: 10.1021/acs.inorgchem.8b02947
Inorg. Chem. XXXX, XXX, XXX−XXX

REFERENCES

(1) Averill, B. A. Dissimilatory nitrite and nitric oxide reductases. *Chem. Rev.* **1996**, *96*, 2951−2964.
(2) Zumft, W. G. Cell biology and molecular basis of denitrification. *Microbiol. Mol. Biol. Rev.* **1997**, *61*, 533−616.
(3) Suzuki, S.; Kataoka, K.; Yamaguchi, K. Metal Coordination and Mechanism of Multicopper Nitrite Reductase. *Acc. Chem. Res.* **2000**, *33*, 728−735.
(4) Lehnert, N.; Dong, H. T.; Harland, J. B.; Hunt, A. P.; White, C. J. Reversing nitrogen fixation. *Nat. Rev. Chem.* **2018**, *2*, 278−289.
(5) Lancaster, K. M.; Caranto, J. D.; Majer, S. H.; Smith, M. A. Alternative Bioenergy: Updates to and Challenges in Nitrification Metalloenzymology. *Joule* **2018**, *2*, 421−441.
(6) Erisman, J. W.; Sutton, M. A.; Galloway, J.; Klimont, Z.; Winiwarter, W. How a century of ammonia synthesis changed the world. *Nat. Geosci.* **2008**, *1*, 636−639.
(7) Fields, S. Global Nitrogen: Cycling out of Control. *Environ. Health Perspect.* **2004**, *112*, A556−A563.
(8) Lehnert, N.; Coruzzi, G.; Hegg, E.; Seefeldt, L.; Stein, L. *Feeding the World in the 21st Century: Grand Challenges in the Nitrogen Cycle*, Arlington, VA, Nov 9 and 10, 2015; National Science Foundation, 2015.
(9) Ferguson, S. J. Nitrogen cycle enzymology. *Curr. Opin. Chem. Biol.* **1998**, *2*, 182−193.
(10) Lehnert, N.; Berto, T. C.; Galinato, M. G. I.; Goodrich, L. E. In *The Handbook of Porphyrin Science*; Kadish, K. M., Smith, K. M., Guilard, R., Eds.; World Scientific: Hackensack, NJ, 2011; Vol. *14*, pp 1−247.
(11) Daiber, A.; Nauser, T.; Takaya, N.; Kudo, T.; Weber, P.; Hultschig, C.; Shoun, H.; Ullrich, V. Isotope effects and intermediates in the reduction of NO by $P450_{NOR}$. *J. Inorg. Biochem.* **2002**, *88*, 343−352.
(12) Zhang, L.; Kudo, T.; Takaya, N.; Shoun, H. Distribution, structure and function of fungal nitric oxide reductase P450nor—recent advances. *Int. Congr. Ser.* **2002**, *1233*, 197−202.
(13) Shimizu, H.; Obayashi, E.; Gomi, Y.; Arakawa, H.; Park, S. Y.; Nakamura, K.; Adachi, S.; Shoun, H.; Shiro, Y. Proton delivery in NO reduction by fungal nitric-oxide reductase. *J. Biol. Chem.* **2000**, *275*, 4816−4826.
(14) Nakahara, K.; Tanimoto, T.; Hatano, K.; Usuda, K.; Shoun, H. Cytochrome P-450 55A1 (P-450dNIR) acts as nitric oxide reductase employing NADH as the direct electron donor. *J. Biol. Chem.* **1993**, *268*, 8350−8355.
(15) Enemark, J. H.; Feltham, R. D. Principles of structure, bonding, and reactivity for metal nitrosyl complexes. *Coord. Chem. Rev.* **1974**, *13*, 339−406.
(16) Franke, A.; Stochel, G.; Suzuki, S.; Higuchi, T.; Okuzono, K.; van Eldik, R. V. Mechanistic studies on the binding of nitric oxide to a synthetic heme-thiolate complex relevant to cytochrome P450. *J. Am. Chem. Soc.* **2005**, *127*, 5360−5375.
(17) Shiro, Y.; Fujii, M.; Iizuka, T.; Adachi, S.; Tsukamoto, K.; Nakahara, K.; Shoun, H. Spectroscopic and kinetic studies on reaction of cytochrome P450nor with nitric oxide. *J. Biol. Chem.* **1995**, *270*, 1617−1623.
(18) Obayashi, E.; Tsukamoto, K.; Adachi, S.-i.; Takahashi, S.; Nomura, M.; Iizuka, T.; Shoun, H.; Shiro, Y. Unique Binding of Nitric Oxide to Ferric Nitric Oxide Reductase from Fusarium oxysporum Elucidated with Infrared, Resonance Raman, and X-ray Absorption Spectroscopies. *J. Am. Chem. Soc.* **1997**, *119*, 7807−7816.
(19) Obayashi, E.; Takahashi, S.; Shiro, Y. Electronic structure of reaction intermediate of cytochrome P450nor in its nitric oxide reduction. *J. Am. Chem. Soc.* **1998**, *120*, 12964−12965.
(20) Lehnert, N.; Praneeth, V. K. K.; Paulat, F. Electronic structure of iron(II)-porphyrin nitroxyl complexes: Molecular mechanism of fungal nitric oxide reductase (P450nor). *J. Comput. Chem.* **2006**, *27*, 1338−1351.
(21) Riplinger, C.; Neese, F. The reaction mechanism of cytochrome P450 NO reductase: A detailed quantum mechanics/molecular mechanics study. *ChemPhysChem* **2011**, *12*, 3192−3203.
(22) Lin, R.; Farmer, P. J. The HNO adduct of myoglobin: synthesis and characterization. *J. Am. Chem. Soc.* **2000**, *122*, 2393−2394.
(23) Buxton, G. V.; Greenstock, C. L.; Helman, W. P.; Ross, A. B. Critical Review of rate constants for reactions of hydrated electrons, hydrogen atoms and hydroxyl radicals (·OH/·O−) in Aqueous Solution. *J. Phys. Chem. Ref. Data* **1988**, *17*, 513−886.
(24) Riplinger, C.; Bill, E.; Daiber, A.; Ullrich, V.; Shoun, H.; Neese, F. New Insights into the Nature of Observable Reaction Intermediates in Cytochrome P450 NO Reductase by Using a Combination of Spectroscopy and Quantum Mechanics/Molecular Mechanics Calculations. *Chem. - Eur. J.* **2014**, *20*, 1602−1614.
(25) Lehnert, N.; George, S. D.; Solomon, E. I. Recent advances in bioinorganic spectroscopy. *Curr. Opin. Chem. Biol.* **2001**, *5*, 176−187.
(26) Beak, P.; Basha, A.; Kokko, B.; Loo, D. The geometry of displacements at nonstereogenic atoms: the formal displacement of alkoxide from alkoxyamines by organolithium reagents. *J. Am. Chem. Soc.* **1986**, *108*, 6016−6023.
(27) Goodrich, L. E.; Roy, S.; Alp, E. E.; Zhao, J.; Hu, M. Y.; Lehnert, N. Electronic Structure and Biologically Relevant Reactivity of Low-Spin $\{FeNO\}^8$ Porphyrin Model Complexes: New Insight from a Bis-Picket Fence Porphyrin. *Inorg. Chem.* **2013**, *52*, 7766−7780.
(28) McQuarters, A. B.; Goodrich, L. E.; Goodrich, C. M.; Lehnert, N. Disproportionation of O-Benzylhydroxylamine Catalyzed by a Ferric Bis-Picket Fence Porphyrin Complex. *Z. Anorg. Allg. Chem.* **2013**, *639*, 1520−1526.
(29) Adler, A. D.; Longo, F. R.; Kampas, F.; Kim, J. On the preparation of metalloporphyrins. *J. Inorg. Nucl. Chem.* **1970**, *32*, 2443−2445.
(30) McQuarters, A. B.; Kampf, J. W.; Alp, E. E.; Hu, M.; Zhao, J.; Lehnert, N. Ferric Heme-Nitrosyl Complexes: Kinetically Robust or Unstable Intermediates? *Inorg. Chem.* **2017**, *56*, 10513−10528.
(31) Paulat, F.; Berto, T. C.; DeBeer George, S.; Goodrich, L.; Praneeth, V. K. K.; Sulok, C. D.; Lehnert, N. Vibrational Assignments of Six-Coordinate Ferrous Heme Nitrosyls: New Insight from Nuclear Resonance Vibrational Spectroscopy. *Inorg. Chem.* **2008**, *47*, 11449−11451.
(32) Sage, J. T.; Paxson, C.; Wyllie, G. R. A.; Sturhahn, W.; Durbin, S. M.; Champion, P. M.; Alp, E. E.; Scheidt, W. R. Nuclear resonance vibrational spectroscopy of a protein active-site mimic. *J. Phys.: Condens. Matter* **2001**, *13*, 7707.
(33) Sturhahn, W. CONUSS and PHOENIX: Evaluation of nuclear resonant scattering data. *Hyperfine Interact.* **2000**, *125*, 149−172.
(34) *CrysAlisPro 1.171.38.41*; Rigaku Oxford Diffraction: Wroclaw, Poland.
(35) *CrystalClear Expert 2.0 r12*; Rigaku Americas and Rigaku Corp.: The Woodlands, TX, 2011.
(36) Sheldrick, G. M. Crystal structure refinement with SHELXL. *Acta Crystallogr., Sect. C: Struct. Chem.* **2015**, *C71*, 3−8.
(37) White, K. A.; Marletta, M. A. Nitric oxide synthase is a cytochrome P-450 type hemoprotein. *Biochemistry* **1992**, *31*, 6627−6631.
(38) Wyllie, G. R. A.; Schulz, C. E.; Scheidt, W. R. Five- to Six-Coordination in (Nitrosyl)iron(II) Porphyrinates: Effects of Binding the Sixth Ligand. *Inorg. Chem.* **2003**, *42*, 5722−5734.
(39) Xu, N.; Goodrich, L. E.; Lehnert, N.; Powell, D. R.; Richter-Addo, G. B. Preparation of the Elusive [(por)Fe(NO)(O-ligand)] Complex by Diffusion of Nitric Oxide into a Crystal of the Precursor. *Angew. Chem., Int. Ed.* **2013**, *52*, 3896−3900.
(40) Xu, N.; Powell, D. R.; Cheng, L.; Richter-Addo, G. B. The first structurally characterized nitrosyl heme thiolate model complex. *Chem. Commun.* **2006**, 2030−2032.
(41) Xu, N.; Richter-Addo, G. B. In *Progress in Inorganic Chemistry*; John Wiley & Sons, Inc., 2014; Vol. *59*, pp 381−446.
(42) Nast, R.; Föppl, I. Über die Bildung von Hyponitrit durch Disproportionierung des Hydroxylamins. *Z. Anorg. Allg. Chem.* **1950**, *263*, 310−315.
(43) Bonner, F. T.; Dzelzkalns, L. S.; Bonucci, J. A. Properties of nitroxyl as intermediate in the nitric oxide-hydroxylamine reaction

DOI: 10.1021/acs.inorgchem.8b02947
Inorg. Chem. XXXX, XXX, XXX−XXX

and in trioxodinitrate decomposition. *Inorg. Chem.* **1978**, *17*, 2487−2494.
(44) Bari, S. E.; Amorebieta, V. T.; Gutiérrez, M. M.; Olabe, J. A.; Doctorovich, F. Disproportionation of hydroxylamine by water-soluble iron(III) porphyrinate compounds. *J. Inorg. Biochem.* **2010**, *104*, 30−36.
(45) Feng, D. W.; Ryan, M. D. Electrochemistry of nitrite reductase model compounds. 3. Formation and characterization of a bis-(hydroxylamine)(tetraphenylporphyrinato)iron(II) complex. *Inorg. Chem.* **1987**, *26*, 2480−2483.
(46) Choi, I.-K.; Liu, Y.; Feng, D.; Paeng, K.-J.; Ryan, M. D. Electrochemical and spectroscopic studies of iron porphyrin nitrosyls and their reduction products. *Inorg. Chem.* **1991**, *30*, 1832−1839.
(47) Quinn, R.; Nappa, M.; Valentine, J. S. New five- and six-coordinate imidazole and imidazolate complexes of ferric tetraphenylporphyrin. *J. Am. Chem. Soc.* **1982**, *104*, 2588−2595.
(48) Walker, F. A. *Handbook of Porphyrin Science*; World Scientific Publishing Co., 2010; Vol. *6*, pp 1−337.
(49) Walker, F. A. Pulsed EPR and NMR Spectroscopy of Paramagnetic Iron Porphyrinates and Related Iron Macrocycles: How To Understand Patterns of Spin Delocalization and Recognize Macrocycle Radicals. *Inorg. Chem.* **2003**, *42*, 4526−4544.
(50) Del Gaudio, J.; La Mar, G. N. Magnetic resonance investigation of the autoreduction of tetraphenylporphinatoiron(III) chloride in the presence of piperidine. *J. Am. Chem. Soc.* **1978**, *100*, 1112−1119.
(51) Zhang, Y.; Hallows, W. A.; Ryan, W. J.; Jones, J. G.; Carpenter, G. B.; Sweigart, D. A. Models for Steric Interactions in Heme Proteins. Structures of the Five-Coordinate Complex Iron(III) Tetraphenylporphyrin Azide and its Six-Coordinate 1:1 Adducts with 1-Methylimidazole and 1,2-Dimethylimidazole. *Inorg. Chem.* **1994**, *33*, 3306−3312.
(52) Lecomte, C.; Chadwick, D. L.; Coppens, P.; Stevens, E. D. Electronic structure of metalloporphyrins. 2. Experimental electron density distribution of (meso-tetraphenylporphinato)iron(III) methoxide. *Inorg. Chem.* **1983**, *22*, 2982−2992.
(53) Grande, L. M.; Noll, B. C.; Oliver, A. G.; Scheidt, W. R. Dynamics of NO Motion in Solid-State [Co(tetraphenylporphinato)-(NO)]. *Inorg. Chem.* **2010**, *49*, 6552−6557.
(54) Scheidt, W. R.; Reed, C. A. Spin-state/stereochemical relationships in iron porphyrins: implications for the hemoproteins. *Chem. Rev.* **1981**, *81*, 543−555.
(55) Scheidt, W. R.; Durbin, S. M.; Sage, J. T. Nuclear resonance vibrational spectroscopy − NRVS. *J. Inorg. Biochem.* **2005**, *99*, 60−71.
(56) Rai, B. K.; Durbin, S. M.; Prohofsky, E. W.; Timothy Sage, J.; Ellison, M. K.; Robert Scheidt, W.; Sturhahn, W.; Ercan Alp, E. Iron normal mode dynamics in a porphyrin-imidazole model for deoxyheme proteins. *Phys. Rev. E: Stat. Phys., Plasmas, Fluids, Relat. Interdiscip. Top.* **2002**, *66*, 051904.
(57) Berto, T. C.; Xu, N.; Lee, S. R.; McNeil, A. J.; Alp, E. E.; Zhao, J.; Richter-Addo, G. B.; Lehnert, N. Characterization of the Bridged Hyponitrite Complex {[Fe(OEP)]$_2$(μ-N_2O_2)}: Reactivity of Hyponitrite Complexes and Biological Relevance. *Inorg. Chem.* **2014**, *53*, 6398−6414.
(58) Reed, C. A. *Electrochemical and Spectrochemical Studies of Biological Redox Components*; American Chemical Society, 1982; Vol. *201*, pp 333−356.
(59) Felton, R. H.; Owen, G. S.; Dolphin, D.; Fajer, J. Iron(IV) porphyrins. *J. Am. Chem. Soc.* **1971**, *93*, 6332−6334.
(60) Phillippi, M. A.; Goff, H. M. Electrochemical synthesis and characterization of the single-electron oxidation products of ferric porphyrins. *J. Am. Chem. Soc.* **1982**, *104*, 6026−6034.
(61) Connelly, N. G.; Geiger, W. E. Chemical Redox Agents for Organometallic Chemistry. *Chem. Rev.* **1996**, *96*, 877−910.
(62) Paulat, F.; Lehnert, N. Detailed Assignment of the Magnetic Circular Dichroism and UV−vis Spectra of Five-Coordinate High-Spin Ferric [Fe(TPP)(Cl)]. *Inorg. Chem.* **2008**, *47*, 4963−4976.
(63) Ikezaki, A.; Ohgo, Y.; Nakamura, M. NMR studies on the electronic structure of one-electron oxidized complexes of iron(III) porphyrinates. *Coord. Chem. Rev.* **2009**, *253*, 2056−2069.
(64) Gans, P.; Buisson, G.; Duee, E.; Marchon, J. C.; Erler, B. S.; Scholz, W. F.; Reed, C. A. High-valent iron porphyrins: synthesis, x-ray structures, π-cation radical formulation, and notable magnetic properties of chloro(meso-tetraphenylporphinato)iron(III) hexachloroantimonate and bis(perchlorato)(meso-tetraphenylporphinato)iron-(III). *J. Am. Chem. Soc.* **1986**, *108*, 1223−1234.
(65) Felton, R. H.; Owen, G. S.; Dolphin, D.; Forman, A.; Borg, D. C.; Fajer, J. OXIDATION OF FERRIC PORPHYRINS*. *Ann. N. Y. Acad. Sci.* **1973**, *206*, 504−515.
(66) Boduszek, B.; Shine, H. J. Preparation of solid thianthrene cation radical tetrafluoroborate. *J. Org. Chem.* **1988**, *53*, 5142−5143.
(67) Carey, F. A.; Hayes, L. J. O-Nitrene and O-nitrenium cation intermediates in reactions of O-substituted hydroxylamines. *J. Org. Chem.* **1973**, *38*, 3107−3114.
(68) Kaba, R. A.; Ingold, K. U. Kinetic applications of electron paramagnetic resonance spectroscopy. 28. N-Alkoxy-N-alkylamino, N-alkoxyamino, and N-alkoxyanilino radicals. *J. Am. Chem. Soc.* **1976**, *98*, 7375−7380.
(69) Malatesta, V.; Ingold, K. U. Kinetic applications of electron paramagnetic resonance spectroscopy. XIV. 1,1-Dialkylhydrazyl radicals. *J. Am. Chem. Soc.* **1974**, *96*, 3949−3954.
(70) Kudo, T.; Takaya, N.; Park, S.-Y.; Shiro, Y.; Shoun, H. A Positively Charged Cluster Formed in the Heme-distal Pocket of Cytochrome P450nor Is Essential for Interaction with NADH. *J. Biol. Chem.* **2001**, *276*, 5020−5026.
(71) Kitagawa, T.; Ozaki, Y. In *Metal Complexes with Tetrapyrrole Ligands I*; Buchler, J. W., Ed.; Springer: Berlin, 1987; pp 71−114.
(72) Burke, J. M.; Kincaid, J. R.; Peters, S.; Gagne, R. R.; Collman, J. P.; Spiro, T. G. Structure-sensitive resonance Raman bands of tetraphenyl and "picket fence" porphyrin-iron complexes, including an oxyhemoglobin analog. *J. Am. Chem. Soc.* **1978**, *100*, 6083−6088.
(73) Paulat, F.; Praneeth, V. K. K.; Näther, C.; Lehnert, N. Quantum Chemistry-Based Analysis of the Vibrational Spectra of Five-Coordinate Metalloporphyrins [M(TPP)Cl]. *Inorg. Chem.* **2006**, *45*, 2835−2856.
(74) Biju, V.; Pan, D.; Gorby, Y. A.; Fredrickson, J.; McLean, J.; Saffarini, D.; Lu, H. P. Combined Spectroscopic and Topographic Characterization of Nanoscale Domains and Their Distributions of a Redox Protein on Bacterial Cell Surfaces. *Langmuir* **2007**, *23*, 1333−1338.
(75) Das, P. K.; Samanta, S.; McQuarters, A. B.; Lehnert, N.; Dey, A. Valence tautomerism in synthetic models of cytochrome P450. *Proc. Natl. Acad. Sci. U. S. A.* **2016**, *113*, 6611−6616.
(76) Hobbs, J. D.; Larsen, R. W.; Meyer, T. E.; Hazzard, J. H.; Cusanovich, M. A.; Ondrias, M. R. Resonance Raman characterization of Chromatium vinosum cytochrome c'. Effect of pH and comparison of equilibrium and photolyzed carbon monoxide species. *Biochemistry* **1990**, *29*, 4166−4174.
(77) Teraoka, J.; Kitagawa, T. Raman characterization of axial ligands for penta- and hexacoordinate ferric high- and intermediate-spin (octaethylporphyrinato)iron(III) complexes. Elucidation of unusual resonance Raman spectra of cytochrome c'. *J. Phys. Chem.* **1980**, *84*, 1928−1935.
(78) Epstein, L. M.; Straub, D. K.; Maricondi, C. Mössbauer spectra of some porphyrin complexes with pyridine, piperidine, and imidazole. *Inorg. Chem.* **1967**, *6*, 1720−1724.
(79) Abu-Soud, H. M.; Silver, J. Mössbauer spectroscopic studies on some low-spin iron(II) and high-spin iron(III) complexes of meso-tetrakis(2,4,6-trimethoxyphenyl)porphyrin. *Inorg. Chim. Acta* **1989**, *161*, 139−141.
(80) Schulz, C. E.; Rutter, R.; Sage, J. T.; Debrunner, P. G.; Hager, L. P. Mössbauer and electron paramagnetic resonance studies of horseradish peroxidase and its catalytic intermediates. *Biochemistry* **1984**, *23*, 4743−4754.
(81) Rittle, J.; Green, M. T. Cytochrome P450 Compound I: Capture, Characterization, and C-H Bond Activation Kinetics. *Science* **2010**, *330*, 933.

DOI: 10.1021/acs.inorgchem.8b02947
Inorg. Chem. XXXX, XXX, XXX−XXX

(82) Stone, K. L.; Hoffart, L. M.; Behan, R. K.; Krebs, C.; Green, M. T. Evidence for Two Ferryl Species in Chloroperoxidase Compound II. *J. Am. Chem. Soc.* **2006**, *128*, 6147−6153.
(83) Debrunner, P. G. In *Mössbauer Spectroscopy of Iron Porphyrins*; Lever, A. B. P., Gray, H. B., Eds.; Physical Bioinorganic Chemistry Series; VCH Publishers, 1989; Vol. 3.
(84) White, C. J.; Speelman, A. L.; Kupper, C.; Demeshko, S.; Meyer, F.; Shanahan, J. P.; Alp, E. E.; Hu, M.; Zhao, J.; Lehnert, N. The Semireduced Mechanism for Nitric Oxide Reduction by Non-Heme Diiron Complexes: Modeling Flavodiiron Nitric Oxide Reductases. *J. Am. Chem. Soc.* **2018**, *140*, 2562−2574.
(85) Abucayon, E. G.; Khade, R. L.; Powell, D. R.; Zhang, Y.; Richter-Addo, G. B. Hydride Attack on a Coordinated Ferric Nitrosyl: Experimental and DFT Evidence for the Formation of a Heme Model−HNO Derivative. *J. Am. Chem. Soc.* **2016**, *138*, 104−107.
(86) Abucayon, E. G.; Khade, R. L.; Powell, D. R.; Shaw, M. J.; Zhang, Y.; Richter-Addo, G. B. Over or under: hydride attack at the metal versus the coordinated nitrosyl ligand in ferric nitrosyl porphyrins. *Dalton Trans.* **2016**, *45*, 18259−18266.

DOI: 10.1021/acs.inorgchem.8b02947
Inorg. Chem. XXXX, XXX, XXX−XXX